Lausten, S., Lund, E., Kühlmeier, L., & Thomsen, O. T. (2014). Development of a High-fidelity Experimental Substructure Test Rig for Grid-scored Sandwich Panels in Wind Turbine Blades. *Strain – An International Journal for Experimental Mechanics*, *50*(2), 111-131. https://doi.org/10.1111/str.12072

Development of a High-fidelity Experimental Substructure Test Rig for Grid-scored Sandwich Panels in Wind Turbine Blades
S. Laustsen, E. Lund, L. Kühlmeier and O. T. Thomsen
Strain - An International Journal for Experimental Mechanics, 2014), Vol. 50, pp. 111 -131
Doi: 10.1111/str.12072

Development of a high fidelity experimental substructure test rig for grid-scored sandwich panels in wind turbine blades

S. Laustsen[1,2], E. Lund[1], L. Kühlmeier[2], O.T. Thomsen[1,3]

[1]Department of Mechanical and Manufacturing Engineering, Aalborg University, Denmark

[2]SE Blades Technology, Denmark

[3]Faculty of Engineering and the Environment, University of Southampton, Highfield Campus, Southampton, SO17 1BJ, UK.

ABSTRACT

This paper outlines high fidelity experimental substructure testing of sandwich panels which constitute the aerodynamic outer shell of modern wind turbine blades. A full scale structural experimental and numerical characterisation of a composite wind turbine blade has been conducted. The development of a full scale numerical model is detailed, and the necessary experimental setup is described. Further, the numerical and experimental results obtained are compared, and an idealised set of boundary conditions for a chosen blade substructure is presented. From this, the development of a test rig suitable for representing the established loading and boundary conditions is presented, and some preliminary experimental results are discussed. The work provides a road map for developing high fidelity experimental substructure tests, which in more generic terms are applicable to similar developments of substructure tests for composite wind turbine blades. Furthermore, recommendations on the use of grid-scored sandwich structures in wind turbine blades are presented, which outline the sensitivity in terms of quasi-static strength to the established loading conditions.

KEYWORDS

Wind Turbine Blades; Experimental Characterisation; Numerical Characterisation; Substructure testing

Correspondence

S. Laustsen, Department of Mechanical and Manufacturing Engineering, Aalborg University, Denmark

E-mail: sla@m-tech.aau.dk

1. INTRODUCTION

Wind turbine blades consist in most cases of laminated composite materials, which are used because of their high strength and stiffness to mass density ratio. Furthermore the blades are most often thin-walled structures, which have a complex exterior geometry due to aerodynamic requirements. Given the complexity of such structures, the structural response is normally evaluated by the use of numerical methods instead of classical analytical methods. Today the most widespread and dominant numerical method is the Finite Element Method (FEM, FE-Method), [1], which has also formed the basis of the numerical analyses performed in this work. To validate the accuracy of the numerical modelling results, the only viable methodology is to conduct an experimental investigation with the objective of correlating the model predictions in terms of displacement and strain fields with the experimental observations. Digital Image Correlation (DIC), [2, 3], has recently become a popular method for obtaining full-field measurements of surface displacements and strains. The DIC method has been utilised in this work to obtain strain fields in the region of interest of a wind turbine blade. Thus, the interface between the numerical and experimental characterisation is the principal interest of the presented work, and the information gathered is used to inform and validate the failure characterisation of a composite wind turbine blade, from the full scale structure, over the laminated substructure, and down to the individual material components.

Numerous structural details exist in modern wind turbine blades, such as ply-drops, discrete stiffeners, adhesive joints and different configurations of sandwich structures. Concerning the latter, sandwich structures are primarily used for the outer shell panels of the blades to increase the buckling resistance and at same time minimising the weight [4]. Even though sandwich structures possess a number of structural advantages, a number of design issues are also introduced with these. Sandwich structures are a special laminated structural assembly comprised of thin laminated composite face sheets with high stiffness and strength separated by a relatively thick, compliant and lightweight core material. The face sheets and the core are adhesively bonded to provide the load transfer between the constituents. Due to this mixture, ideally for sandwich structures/panels loaded in transverse shear and bending, the face sheets are intended to transfer the in-plane normal and shear stresses, while the core carries the through-thickness shear stresses. Depending on the application and structural use situations might occur, where the sandwich structure is not loaded ideally. Stress concentrations from production defects or ply-drops in the face sheets may introduce parasitic stress components, which can jeopardise the structural integrity. Further, localised loads may induce through-thickness normal stresses, which induce severe loads into the core material and the interface between the core and face sheets. Thus, with the increasing use of sandwich structures closer to the primary load paths of the blades, together with their well known sensitivity to stress concentrations arising from

production defects or through-thickness effects due to localised loads or ply-drops, accurate failure prediction becomes of even more critical importance.

Failure characterisation of composite structures, both monolithic and sandwich laminates, is rarely straightforward due to their complexity and receives widespread attention throughout the research community [5]. For the case of sandwich structures, these can in most cases be reliably investigated numerically with respect to their stiffness response for even very complex load cases. However, the prediction of failure - either initiation or complete - is computational very difficult and must in most cases be supported by experimental investigations [6, 7]. However, the experimental failure analysis for both the static load case and in fatigue is most often only realised as coupon test specimens subjected to simplified one-dimensional loading conditions, either due to practical restrictions in the test setup or unknown loading conditions occurring from the structural response of the global structure. Thus, these simplified tests rarely agree with the actual loading conditions, which are usually multi-dimensional. Superposing the one-dimensional cases do in some cases correspond well to the simulated response of a multi-dimensional case, but for other cases where e.g. failure modes interact this will not be the case. To accurately characterise the structural responses and the failure loads of specific substructures, the displacement, stress and strain field distributions are normally investigated. As explained in [8], complex numerical models can be developed for the global structure, and based on a parent/child like link, detailed submodels of critical subcomponents can be established from which even further detailed submodels can be built etc. Such modelling efforts allow identification of critical regions on all modelling levels, but they also allow an efficient approach to translate induced global loads into local loads and boundary conditions for a given subcomponent. Ideally, the submodelling approach in combination with accurate (phenomenological or physically based) predictive failure models can be utilised to estimate failure from either a top-down or a bottom-up approach, respectively. The top-down approach primarily enables the prediction of structural (stiffness driven) failure phenomena (e.g. buckling), while the bottom-up approach primarily facilitate prediction of material component (micro-structure) failure (e.g. excessive stresses or strains). The approach as described could be very useful, but due to the fact that the predictive failure models are often based on simplified tests, and also that even very detailed computational models are always based on a specific set of simplifying assumptions, the different levels of analysis will almost always display a certain mismatch. Thus, experimental characterisation on the substructure level should ideally be conducted to account for these uncertainties. Depending on the required substructure level to test (ranging from full scale structure to material test), cost and time obviously are influential factors in the decision making as well. Thus, in practice the approach that is often taken for the development of wind turbine blades is to only conduct simplified tests in combination with structural numerical models. Ultimately, the wind turbine blade structure

is subjected to a full scale experimental characterisation to validate the strength margin of the structure. The choice of sacrificing the substructural experimental investigations does not only imply the risk of enforcing a very conservative design. Since the developed design has not been experimentally validated before the final full scale test, there is also a risk that failure occurs at this stage, meaning the final and most costly phase of the development process has to be redone.

The basis of this work is a full scale experimental and computational characterisation of a complete wind turbine blade to obtain detailed information about the displacement, strain and/or stress boundary conditions of a chosen substructural zone (or substructure). This information will be utilised as the basis of facilitating further and more detailed experimental investigations on the substructure level, which will be conducted in a multiaxial test rig designed to take the actual loading and boundary conditions into account. The chosen substructure for this work is a multiaxially loaded grid-scored foam cored sandwich panel cut out of the aerodynamic shell of a commercial wind turbine blade. The multiaxial substructure test rig is discussed wrt. design and validation, and it is demonstrated how failure observations, which cannot be realised from simplified uniaxial tests, can be translated into blade design recommendations. The paper is concluded by a discussion, which argues that the methodology presented provides a roadmap for how high fidelity substructure tests for wind turbine blade structures can be conducted.

2. SELECTION OF BLADE SUBSTRUCTURE

Modern wind turbine blades are typically manufactured using a combination of monolithic and sandwich composite materials. The (outer) aerodynamic shells and the internal stiffeners (shear webs) are typically made as lightweight composite sandwich structures, whereas the root end and the central blade main laminates (girders) on both the pressure and suction sides are thick-walled monolithic composite laminates. The different structural components and the terminology used with respect to the wind turbine blade are shown in Figure 1. The requirements for the aerodynamic shell of the wind turbine blades often dictate that the sandwich structures should have a single or double curved geometry, which implies that the materials in the production process of the sandwich structure need to be draped to follow the geometry. This is usually not a problem for the face sheets, since these are made of thin layers of glass or carbon fibre fabrics, but the core materials are usually delivered as thick plates of foam (or balsa wood), which cannot be fitted directly to the geometry. To accommodate for this, the materials are cut in small blocks and attached to a thin carrier fabric, which can be draped. This type of core is known as ”grid-scored”, see Figure 2. If the manufacturing process is based on resin transfer moulding, which is the typical production method for wind turbine blades, resin passes through these scores, thus creating a resin grid within the foam material. This specific core configuration together with the face sheets is referred to as a

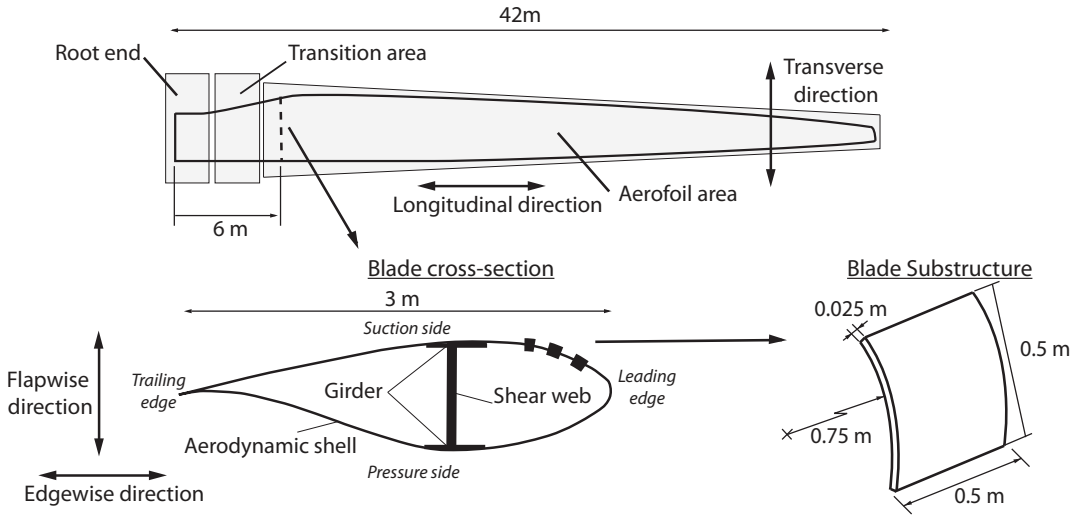

Figure 1. Terminology and location of the substructure of interest

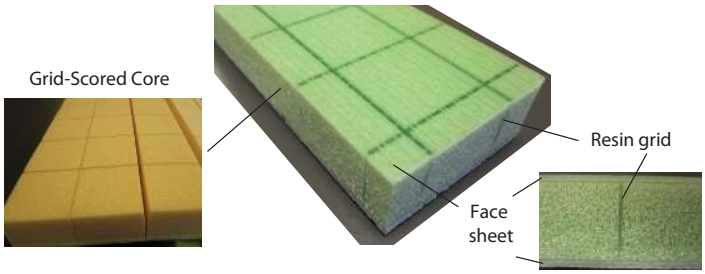

Figure 2. The grid-scored sandwich structure

grid-scored sandwich structure. The focus of the present work is a foam cored grid-scored sandwich structural element, henceforth referred to as the sandwich substructure, representing an element of the aerodynamic shell of a commercial wind turbine blade, see Figure 1. Since the resin in situ the foam core is much stiffer than the foam, the presence of the grid will affect the local stiffness and load transfer of the core material. This in turn changes the stress distribution locally, and induces local stress concentrations in the interfaces between the different constituents, which may lead to failure. The sandwich substructure, which is investigated in this work is located 6 meter from the root end, see Figure 1. This particular substructural element and its location has been based on some general concerns related to the performance of grid-scored sandwich elements in highly loaded areas of the blade. As shown, the root end of the blade is connected to the aerofoil area through a transition zone. The root end consists of thick-walled monolithic composite laminates, while the aerofoil primarily is made of sandwich structures except for the girders. In the transition area, as the name implies, a transition from monolithic to sandwich laminate exists, and the sandwich panel in the aerofoil area closest to the transition

area has been chosen as the object of this study. At this location the local loading conditions are not influenced by the geometric transition. Furthermore, the global bending deformation mode of the blade induces the most severe local loads adjacent to the root end. As highlighted by the dashed line in Figure 1, only a part of the cross-section is investigated. The chosen sandwich substructure constitutes the suction side of the aerodynamic shell between the girder and the leading edge. This substructure is of particular interest due to the presence of high in-plane compressive forces in the longitudinal blade direction, and these in combination with transverse constraint and ovalisation effects in the blade cross section plane induce complex biaxial loading conditions in situ the grid-scored sandwich core and the face sheets. A premature failure scenario of the structure when subjected to these loading conditions is very critical since the blade might loose a significant part of its load carrying capacity.

The grid-scored sandwich configuration has been studied in a more generic form for the case of core junctions in sandwich structures. Here the term junction refers to an intersection, where the core stiffness and strength properties change discontinuously. In practice, this type of structural feature is typically associated with a change of core material, for example from a low density to a high density polymer foam core. Recently, the generic core junction case has been the subject of significant research, as reported in eg. [9] and [10]. However, the generic core junction case does not accurately describe the grid-scored core case, as the interactions between the core, resin grid and face sheets for this case are more complex. In particular, the overall load/stress redistribution, the locally induced stress concentrations and the characteristic decay lengths of the local effects, induced by the presence of a resin grid in the compliant core, are significantly different than for the generic core junction case. Further, the aim of this research is to investigate the failure behaviour when the structure is subjected to loading conditions that are realistic for wind turbine blade, i.e. multiaxial loads in this case.

3. FULL SCALE CHARACTERISATION OF WIND TURBINE BLADE

To determine the local loading conditions of the chosen sandwich substructure, a full scale characterisation of a wind turbine blade subjected to static loading conditions has been performed. The global loading conditions that cause the most severe loads on the substructure have been selected, as shown in Figure 3. The primary loads on a wind turbine blade comprise of transverse bending from aerodynamical lift in the flapwise direction and aerodynamical drag and gravity forces in the edgewise direction. The combined flapwise and edgewise forces are used to generate two load cases, where the selected grid-scored sandwich substructure is subjected to direct compression and tension loads, respectively. Each load case has been named according to the direction and sign convention as shown in Figure 3, except for the combined cases, which refer to the state of stress in the substructure. The choice of load cases has been determined by the loading

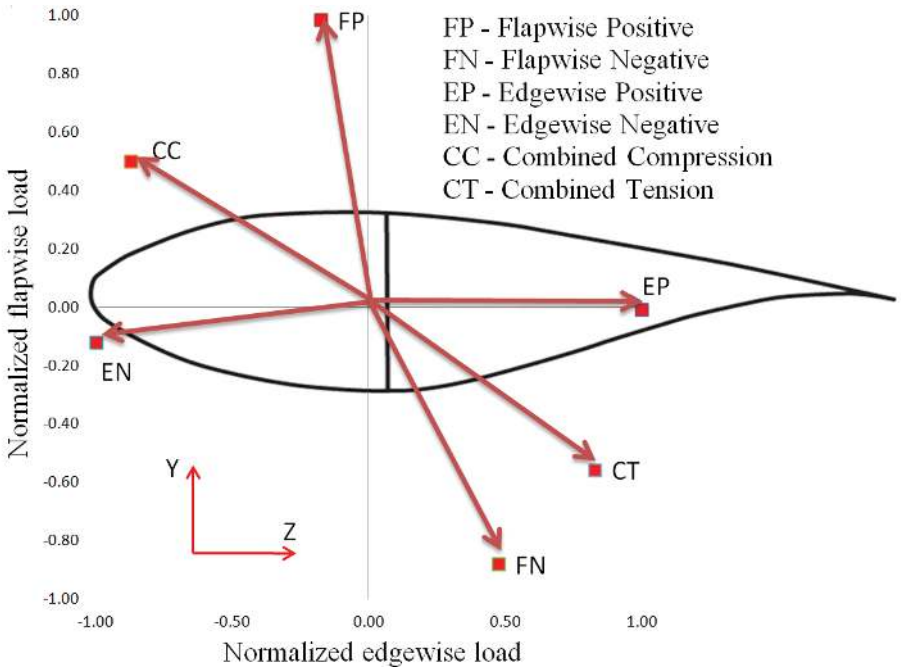

Figure 3. Imposed global loading conditions

envelope that could be realised in the full scale test rig experimental setup. Thus, only a certain number of load cases with limited amplitudes could be realised. To investigate the response at higher amplitudes the numerical model was used as detailed in Section 3.3. Further, as shown in Figure 3, combined loadings were realised although pure edgewise and flapwise loadings were ideally desired. The main reason for this was insufficient transverse loading capacity in the control scheme of the actuators, which should otherwise compensate for the bending coupling effects in the blade.

3.1. Full scale experimental setup

The framework of the full scale experimental setup has determined the imposed loading conditions, deformation monitoring, and blade design that is used as reference for the present work. The measurements performed and the conditions of the full scale characterisation are explained in the following. The full scale experimental setup is shown in Figure 4. The tested blade is a 42 meter long composite wind turbine blade, and for the testing it was clamped to a root end fixture and loaded by a double station hydraulic actuator setup corresponding to inner and outer load introduction points, respectively. As seen in Figure 4, the blade tip had been removed, and the outer load introduction point was located 31 meters from the root end. In combination with the inner load introduction at 17 meters, the sandwich panel selected for the substructure tests could be loaded in a manner that closely resembles the operational conditions.

Figure 4. Full scale blade test setup

The blade displacements and strains were measured during the testing. First of all, the displacement at the outer load introduction point was monitored to achieve a global representation of the blade stiffness. Secondly the exterior surface of the blade in the region of the sandwich substructure was monitored. The measurements were performed using Digital Image Correlation (DIC) [2, 3]. The camera setup and the blade surface with a spray painted speckle pattern are shown in Figure 5. As shown, the DIC setup used is a stereo or 3D setup, which accommodates for measurement of both in-plane

Figure 5. DIC setup and the instrumented region of interest

and out-of-plane surface displacements. DIC was used to measure the displacement field on the surface of the sandwich substructure, and this was subsequently used to derive the in-plane strain field on the surface. To validate the measured strains, the surface was instrumented with strain gauges on the outer blade surface. In addition strain gauges were mounted on the inner side of the substructure to give a measure of the through-thickness variation of the in-plane strains. Finally, adjacent to the selected sandwich substructure, a cross section of the blade was mounted with displacement transducers (LVDTs) to monitor the relative deformation (ovalisation) of the section. More LVDTs were mounted in the vicinity of the selected sandwich substructure to obtain information about the bending behaviour of the panel, see Figure 6.

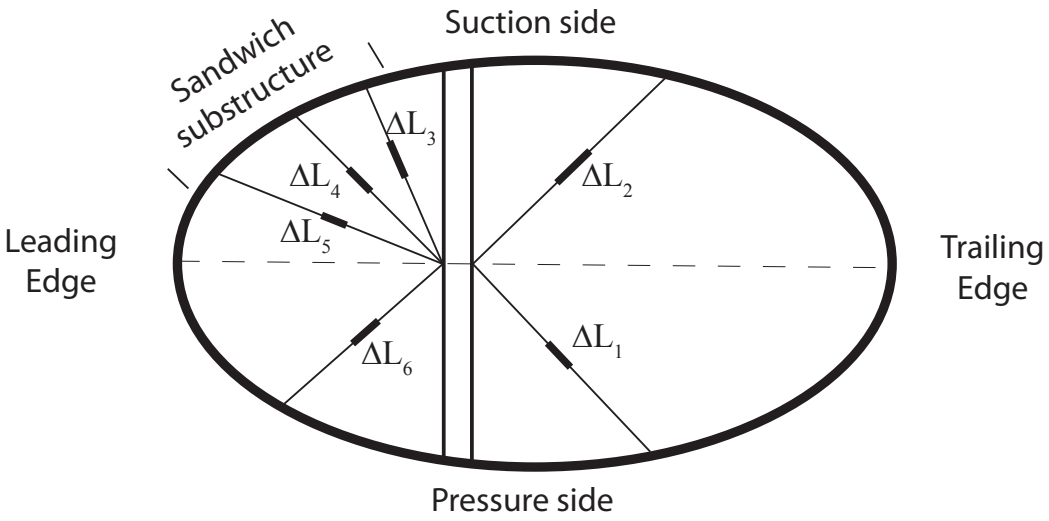

Figure 6. Displacement sensor setup of the blade cross section

3.2. Full scale geometrical nonlinear numerical model

Analysis of large FE models of thin-walled laminated composite structures like wind turbine blades are often computationally expensive because of the many material layers involved, and because of the geometrical nonlinearities involved in the presence of relatively large deflections. In analysis of thin-walled structures, degenerated solid elements [11] also referred to as equivalent single layer (ESL) shell elements are most often used, because of their modelling and solution efficiency compared to solid elements. Because of this, much research and development of shell formulations has been done through the years in terms of making the elements as solution accurate as possible, e.g. by stabilisation techniques that circumvent the locking effects in the isoparametric shell formulations [12], and the treatment of shell normals [13].

The blade structure in the present work was modelled with the four node ESL shell element in MSC Nastran. The model is shown in Figure 7 to provide a visualisation of the blade geometry and the chosen discretisation. The model is discretised

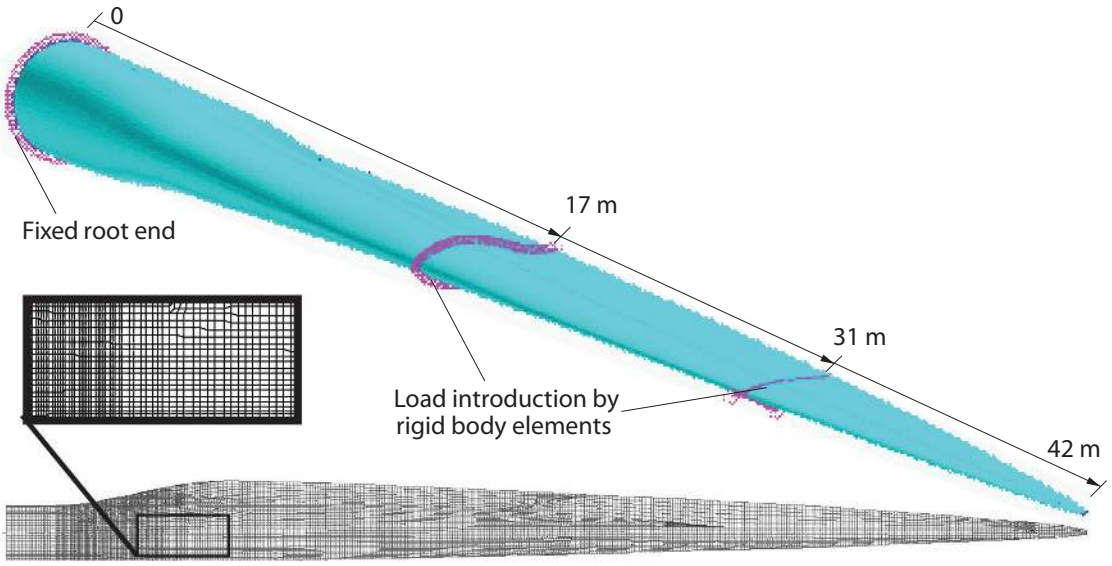

Figure 7. The Finite Element model of the blade structure

into approximately 40,000 elements, which correspond to nearly 230,000 Degrees of Freedom. The stacking sequence in the elements ranges between one and 100 laminae to correctly describe the constituents of the blade. The discretisation, as in any other FEM model, has to be chosen properly to ensure convergence. In this case, however, the discretisation is not only driven by a demand for model convergence, but rather by the desire to have a good representation of the stiffness variation. The lay-ups do in some cases change down to a length of 10 mm, while the convergence demands in terms of global strain energy might be element sizes 10 or 100 times longer than that. This also explains the high number of degrees of freedoms for the current model. To represent the load introduction in the experimental setup (see Figures 4, 5 and 7), rigid body elements have been used to distribute the applied model load to two cross sections of the blade. This caused the cross sections, through which the external loads are applied, to be completely rigid, and this is assumed to correspond well with the load blocks used in the experimental setup. The localised effects from the load introduction points were not found to have an effect on the strain and stress fields in the region of interest (sandwich substructure), as these are located far away from the loading sections. In order to account for geometrically nonlinear behaviour, the FE analysis utilised a step-wise Newton-Raphson solution method. Thus, large displacements and rotations were taken into account. Only small strains were assumed, and hence only linear constitutive relations were used. The geometrical description of a wind turbine blade often conveniently relates to its external surface, and node offset options are normally used to account for

this. As explained in [14], node offsets can sometimes lead to erroneous results. This is especially the case when torsional or coupled bending-torsion responses are considered. This has been taken into account in the blade analyses conducted in this work, where coupling effects between the bending and torsional deformation modes exist due to the geometry and constituents of the blade.

3.3. Full scale results

From the full scale numerical model and the experimental measurements a set of global and local deformation results was obtained for each global blade load case. The results enable the mapping of the local loading and boundary conditions experienced by the selected sandwich panel. This was done through identification of the most dominant stress and strain components in the panel, which were subsequently idealised and generalised. Local results have been derived for the selected sandwich substructure, but the global measures of the deformed blade configuration have also been compared. The blade tip deflection and the relative cross section deformations have been used to validate that the numerical model predictions correspond satisfactorily to the experimentally observed data. Such a correlation should preferably be performed based on displacements rather than on the strains. In the numerical model the strain field computed based on the displacement field is normally very smooth, while the experimentally obtained strain field will typically appear to contain significant noise caused by measurement scatter and issues with spatial resolution. Although strain gauges can provide an accurate measurement of the surface strains, the strain variation across the blade surface can be influenced by local geometric imperfections (induced in the manufacturing), which cannot realistically be included in a global FEM model. Effects of such local geometric variations will typically not give rise to equally significant discontinuities in the displacement field. Thus, experimentally obtained displacements will in most cases be a more useful reference for comparison, although it is the strains that are really the desired objects for comparative studies and detailed analysis. The relative cross section deformation was measured to develop a quantitative understanding of the deformation state of the considered sandwich substructure. A comparison between the numerically predicted and the measured cross section deformations is shown in Figure 8. It is seen seen that the predicted and measured displacements follow very similar trends, but it is also clear that significant deviations between the two data sets are present. In this connection it is important to underline the many uncertainties that are likely to have influenced the measurements. One source to the observed deviations is the geometrical and constitutive discrepancies that exist between the numerical model and the real structure. However, for the comparison in Figure 8, the most important factor believed to be responsible for the significant high relative deviations between the measured and predicted cross section deformations is the relatively small values of the displacements. The

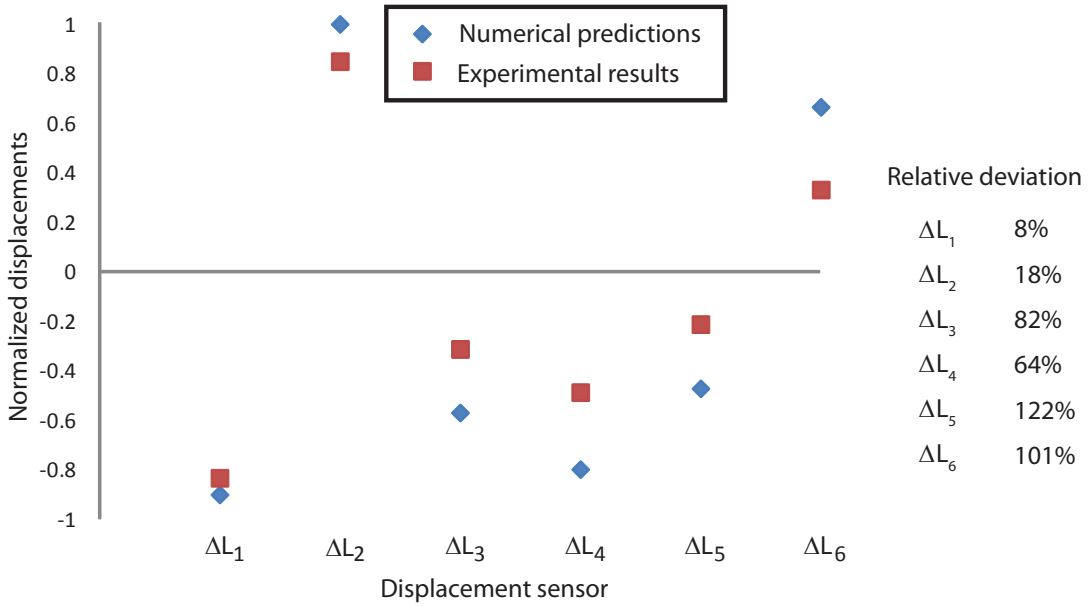

Figure 8. Displacement sensor comparison for the flapwise positive (FP) load case

relative measure becomes very sensitive to even small physical discrepancies between the displacement values. Thus, it is assessed that although large numerical deviations exist, the numerical model represents the localised deformation behaviour of the blade reasonably well. Another important thing to note for the ovalisation results is the rather unusual occurrence that the experimental results show that the actual blade is stiffer than the numerical model. For most experimental versus numerical cases it is opposite. In the present case the measured cross section deformations directly reflect the chordwise stiffness of the blade. Since the blade considered had gone through considerable repairs possibly due to production defects these repairs could have influenced the chordwise stiffness. This in combination with the relatively small displacement values measured could have made the actual blade stiffer than the numerical model. Another possible explanation is the occurrence of a flexible (instead of a fixed) boundary condition at the root end. A small flexibility will result in a larger rigid body motion of the blade, which causes less deformation of the blade cross section.

3.3.1. Local stress and strain results

The local stress and strain fields of the selected sandwich panel constitute the basis for determining the loading conditions, which need to be replicated in the substructure test. The computed and measured strain fields of the exterior surface of the sandwich substructure are shown in Figure 9. As mentioned, the substructure was instrumented with strain gauges in the area where DIC measurements were conducted. The strain gauge readings are included by the coloured dots

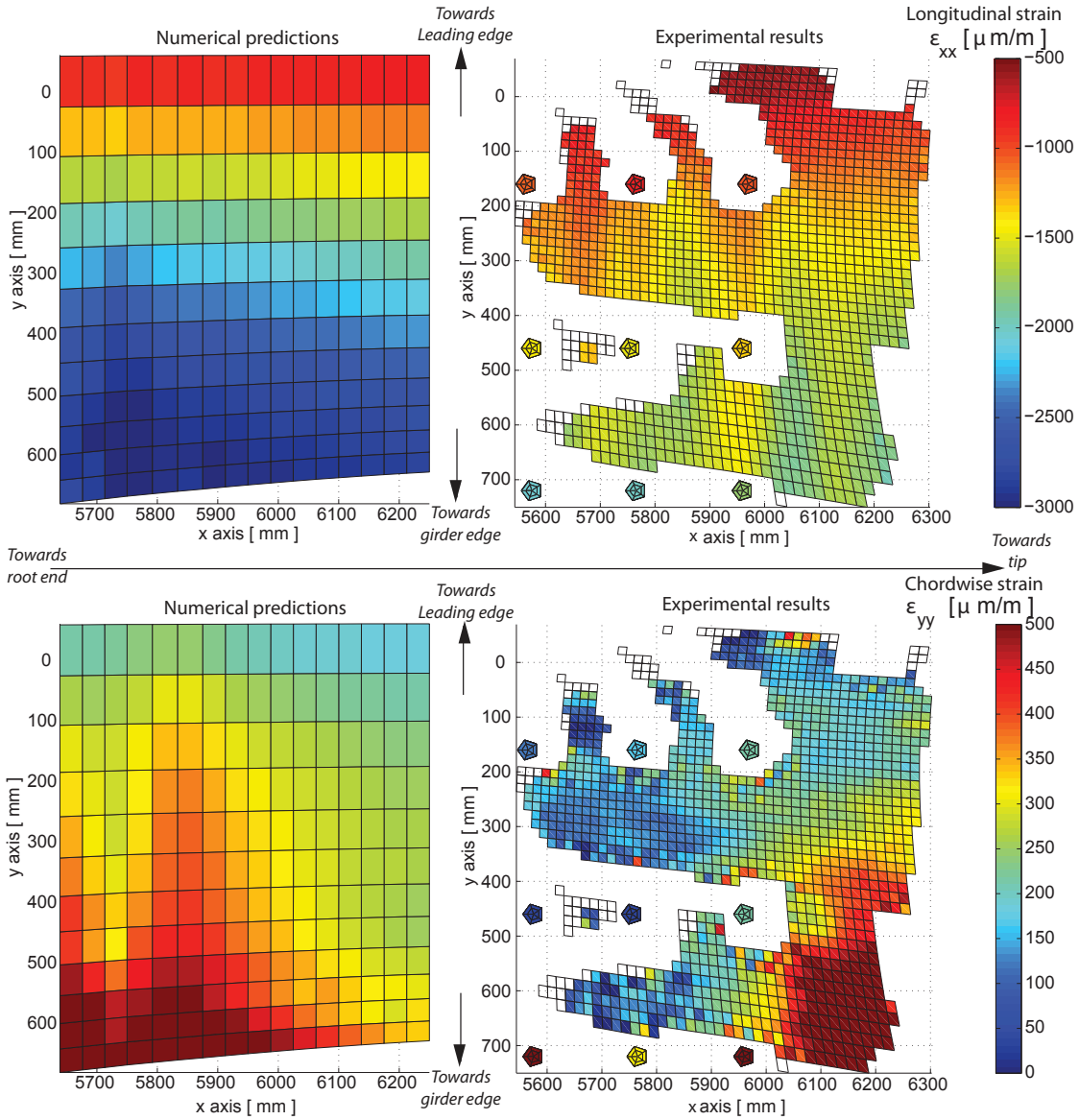

Figure 9. Numerical predicted and experimentally obtained surface strain field in chord (y) and lengthwise (x) directions of the blade for the FP load case. (dimensions reference is given to Figure 1)

shown overlayed on the experimental DIC results. Overall the experimental results (strain gauge and DIC measurements) agree well with each other, although some discrepancies are seen for the strains in the chord direction (ε_{yy}) close to the girder edge. The predicted and experimentally obtained strain fields display very similar trends and levels of magnitude, albeit some discrepancies are clearly observed as well.

Overall, the numerical model is found suitable for obtaining the sought characteristic boundary conditions of the selected sandwich substructure. From the analyses it has been observed that the normal strains in the longitudinal direction (ε_{xx}),

which are due to the global blade bending, are by far the largest strain components for all load cases. Due to the rather crude spatial resolution of the DIC measurements, see Table I, the best agreement between numerical and experimental data with regards to distribution and magnitude was found for the flapwise positive (FP) load case. It was further observed that the shear strain field and the principal strain directions show that the chordwise and longitudinal strains closely represent the minor and major strain component axes, respectively. Since the experimental characterisation was realised at a load

Table I. Specification of the DIC data

Technique used	*Stereo Image Correlation*
Subset size	40 x 40 pixel
Shift	40 pixel (0 % overlap)
Camera	8 bit, 2048 x 2048
	ARAMIS 4M system
Field of view	750 mm x 750 mm
Measurement points	1485
Displacement	
Spatial resolution	21 mm
Resolution	5 μm
Strain	
Smoothing method	Averaging (7x7) ARAMIS
Differentiation method	Numerical
Spatial resolution	126 mm
Resolution	80 μm/m

level within the normal operation conditions of the blade, the applied loading conditions were significantly lower than the failure load levels of the blade. Thus, the numerical model appears to be reasonably accurate for the load levels representing normal operation conditions, and it is further assumed that it will be valid for arbitrary loading directions and magnitudes. This allows for a further investigation of the stress and strain response of the substructure at higher load levels, albeit the accuracy of the FE model has not been validated at load levels close to the limit state. As explained previously, the sandwich substructure was found to be subjected to the largest strains in the longitudinal direction for all load cases. Furthermore, the numerical model results together with the strain gauge measurements conducted on the exterior and

interior sides of the panel indicate that almost no variation through the panel thickness existed in that direction. In the chordwise or transverse direction, the geometrically nonlinear analyses and the ovalisation measurements obtained using the displacement sensors shown in Figure 10 indicate an increasing level of bending deformation in the chord direction as the load level increased (shown from the deformation trends outlined by the red and green dashed lines for the 300% FP and 300% FN load case respectively). This is also confirmed by the stress results, which change from a uniform distribution to a bending-like distribution through-thickness of the sandwich shell, see Figure 10, which again indicates that cross section ovalisation occured due to the Brazier effect [15]. Although, the nonlinear model predictions indicate that increasingly

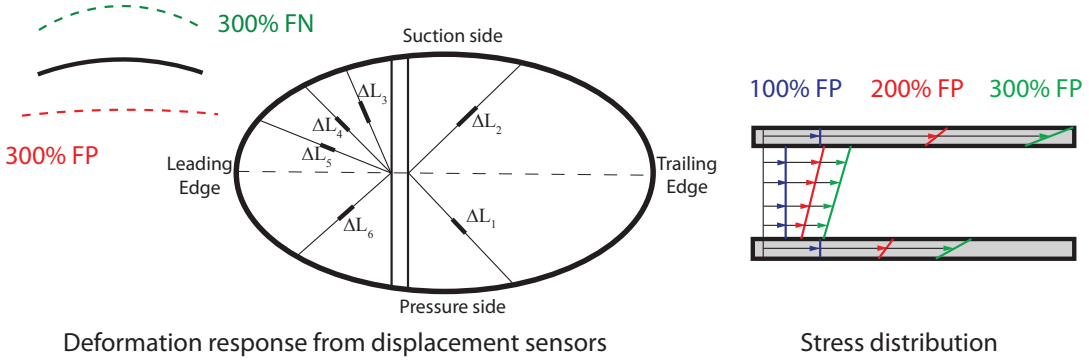

Figure 10. Deformation behaviour and stress distribution in the sandwich substructure in the chordwise blade direction

non-uniform in-plane stresses were building up in the chordwise direction with increasing longitudinal strain, see Figure 10, the relationship between the two quantities corresponded mostly to the Poisson's ratio of the laminate. Thus, the results suggest that a certain amount of constrained transverse contraction exist. From this the overall bending response was found to depend nonlinearly on the amplitude of the applied load, indicating that geometrically nonlinear interaction effects were coming into effect at the highest investigated load level (300% load cases).

3.3.2. Idealisation and generalisation of the local loads

Based on the stress and strain fields obtained from the full scale nonlinear finite element model, an idealised set of boundary conditions is proposed. The loading conditions and displacement constraints, which are aimed to be realised for the selected grid-scored sandwich substructure, are shown in Figure 11, where P_L is a longitudinal (lengthwise blade direction) in-plane load (or the load in the flat direction of the panel), P_T is a transverse (chordwise blade direction) in-plane load (or the load in the curved direction), and M is a pure bending moment in the transverse direction. Furthermore, the displacement constraints are shown w.r.t. the (x,y,z)-coordinate system. An overview of the dependency of the loading

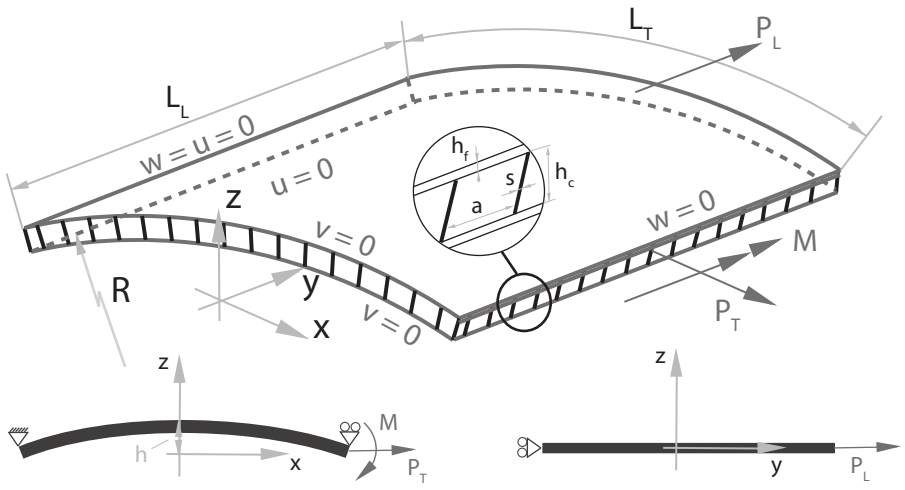

Figure 11. Local loading conditions and displacement constraints shown for the sandwich substructure

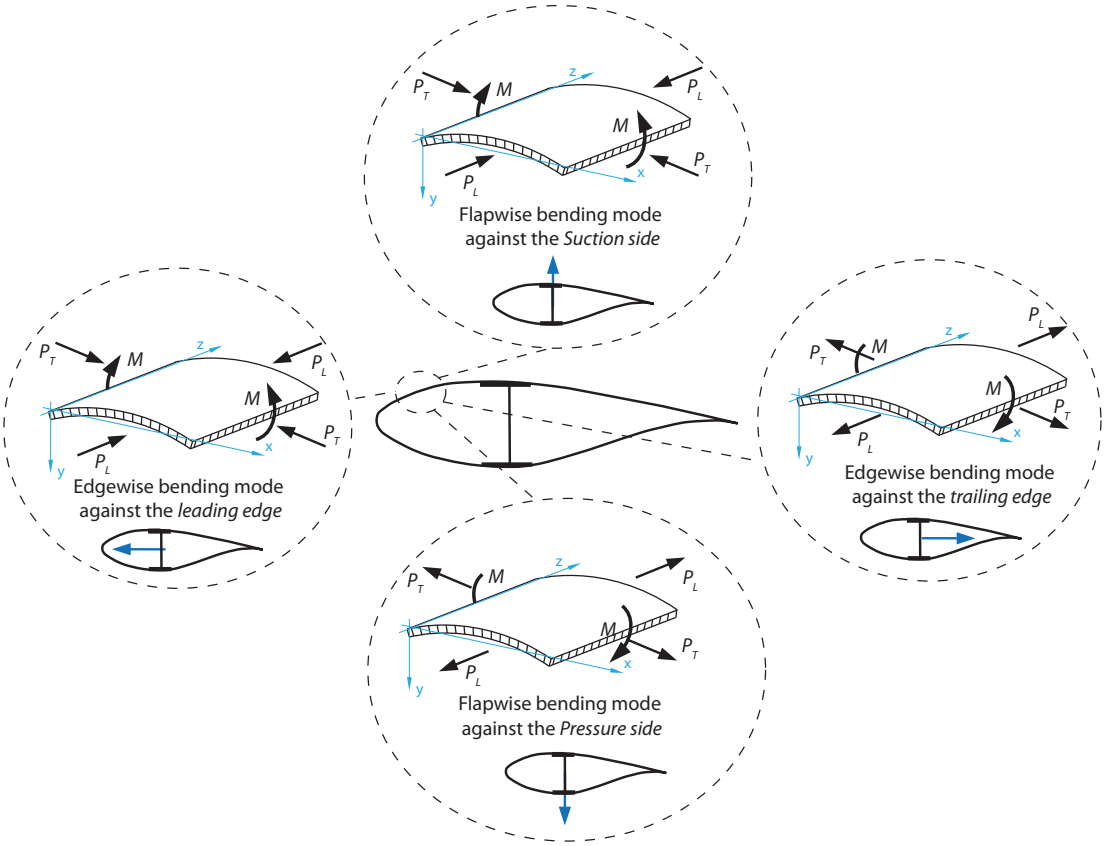

Figure 12. Visualisation of the relationship between the global blade deformation modes and the local panel loads

conditions on the global blade deformation mode is schematically shown in Figure 12 and can be interpreted in the following way:

- Tension/compression forces (P_L) occurring in the longitudinal direction of the blade due to the global blade bending deformation mode
- Constrained contraction/expansion leading to tension/compression forces (P_T) in the transverse direction occurs due to Poisson's ratio effects and due to the closed box cross-section design
- Bending moments (M) in the chordwise direction due to ovalisation of the cross-section with increasing levels of P_L.

To investigate the load components dependency on each other and their influence on the internal stress distribution in the sandwich structure a local full 3D FE model, as shown in Figure 13, has been made. The idealised FE model was

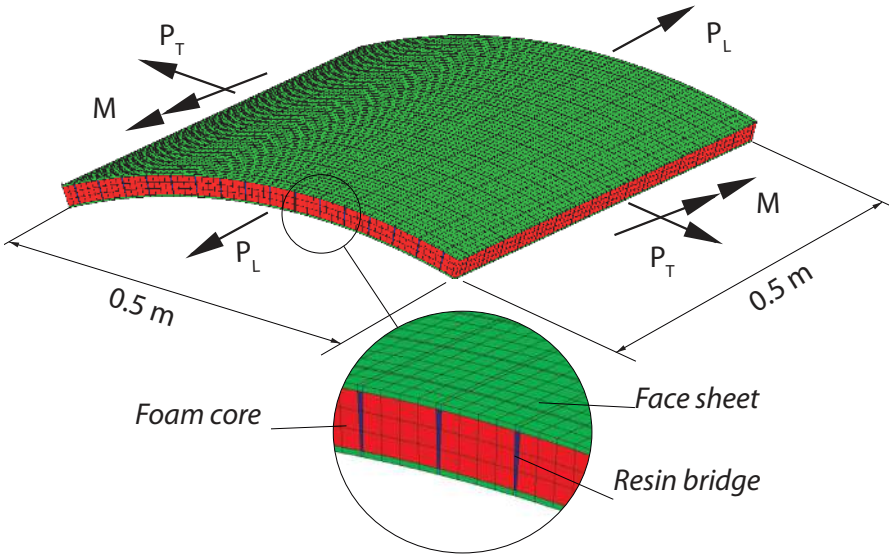

Figure 13. Solid FE model of the idealised sandwich substructure

discretised by 34,000 eight node solid elements in MSC Nastran. The model was chosen only to facilitate linear predictions since indicative magnitudes of the three load components (P_L, P_T and M) were desired. Thus, the predictions was used to outline the basic load requirements for the multiaxial test rig, which need to be fine tuned depending on the specimen design. A simplified shell model would also have been suitable for the explained purpose but in order to investigate the localised load distribution due to the resin grid a solid model was chosen.

The dependency of transverse load P_T on the longitudinal load P_L and the bending moment m on the transverse load P_T are shown in Figures 14 and 15. The magnitudes of the load components were obtained from the full scale geometrical nonlinear model, which can predict the node reaction forces, for the experimentally realised load levels (lowest data points) and the 200% and 300% load levels (the two subsequent data points). The load magnitudes were further applied to the local full 3D FE model to investigate possible prediction discrepancies. Generally non were discovered although linear and geometrical nonlinear predictions were compared. A possible explanation to this is shown by the comparative load plots (Figures 14 and 15). It is important to notice that the results shows that the relationships between P_L and

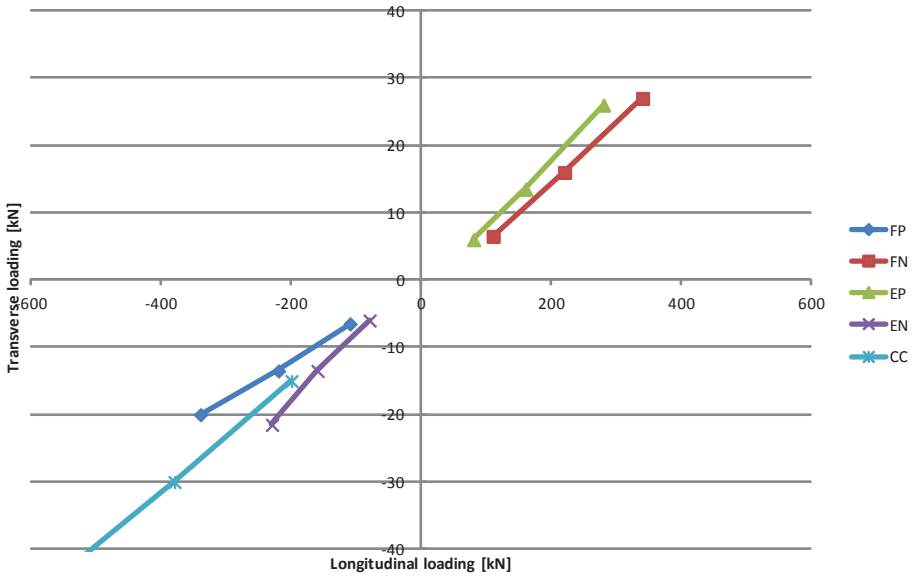

Figure 14. Relationship between the longitudinal load component P_L and the transverse load component P_T

P_T, and P_T and M are approximately linear. Thus, nonlinear effects (compared to applied load) on full scale level can in this case be modelled by linear assumptions. It is further noticed that the dependency is approximately the same for the different deformation configurations of the blade. This means that only two panel deformation configurations need to be realised experimentally to represent the local loading conditions in the blade independently of the different global loading conditions; one tension-tension-bending case and one compression-compression-bending case. If a more generic failure investigation is desired, the failure behaviour corresponding to different combinations of the three load components P_L, P_T and M should be investigated. Based on the reasoning presented above it has been decided to limit the possible loading scenarios of the multiaxial substructure testing facility to the combinations illustrated in Figure 12. This choice implies some limitations to the actual loading conditions that may be imposed in the testing, but at the same time numerous combinations of P_L vs. P_T, M relationships corresponding to rather general and realistic substructure loading conditions

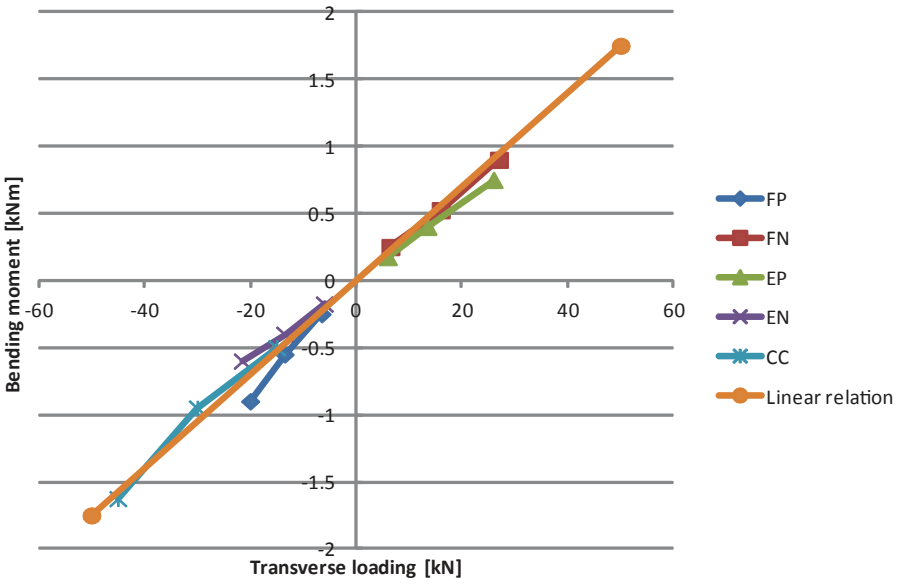

Figure 15. Relationship between the transverse load component P_T and the transverse bending moment M

can be simulated. The linear dependency of the bending moment M on the transverse load P_T has caused an essential design choice for the test rig developed in this work. Thus, the transverse bending moments applied to the sandwich specimen must be linearly dependent on P_T:

$$M = kP_T \tag{1}$$

where k is a constant. The limitation is shown in Figure 15. The explained limitation, others as well and the practical aspects of the design and commissioning of the multiaxial test rig will be addressed further in the next section.

4. SUBSTRUCTURE CHARACTERISATION

From the numerical and experimental full scale wind turbine blade characterisation presented in the preceding sections, the dominant local loading components and their respective relations and magnitudes have been identified. This enables further and more detailed experimental investigations of the selected sandwich substructure. Before experimental realisation efforts are made it is appropriate to consider if any geometrical simplifications can be made. The reason for this is primarily to simplify the specimen producibility, but also to reduce the required modelling efforts. As indicated in Figure 11 the chosen substructure geometry is a sandwich panel idealised as a cylindrical shell, which implies a singly curved geometry.

To accommodate for different substructure panel configurations located at different positions in the blade a number of design parameters have been identified:

- Radius of curvature
- Face sheet thickness, inner side
- Face sheet thickness, outer side
- Core thickness
- Length of core block, longitudinal (flat) direction
- Length of core block, curved direction
- Score width
- Panel length
- Constitutive properties of the different constituents (face sheets, resin, core)

As stated previously, the objective of this work is to enable failure characterisation for a specific sandwich substructure element taken from an arbitrary location of the aerofoil shell of a wind turbine blade. All the parameters listed above may significantly influence the failure envelope corresponding to the three load components P_L, P_T and M (Figure 11). Thus, the outlined parameters have been taken into account in the development of the test rig and the associated specimen geometry and constitution, to accommodate for possible future investigations of the generic failure behaviour of grid-scored sandwich panels (e.g. panels with different radii of curvatures).

4.1. Test rig design

The test rig shown schematically in Figure 16 has been developed and realised in this work. The main (vertical) load frame and actuator is a uniaxial servo-hydraulic 400 kN (Schenck - Hydropuls® PL 400) testing machine, which has been extended with an additional horisontal 63 kN actuator (Instron - Hydropuls® PL 63) and associated loading frame. The test setup further involves a roller support table, which allows the frame of the horisontal actuator to move freely hence avoiding interaction of the two actuators. The specimen is realised as a cruciform-like specimen and positioned in the centre of the test rig. The 400 kN actuator in the uniaxial testing machine provides the longitudinal load component, P_L, and is shown separately in Figure 17. This part of the setup is comparable to a simple uniaxial tension/compression test setup, as shown from the free body diagram in Figure 17. The additional horisontal actuator including the loading frame is shown in Figure 18. These parts provide the two remaining load components, i.e. the transverse force P_T and the bending moment M, respectively. As shown in Figure 18 the transverse loading system is a symmetric design consisting

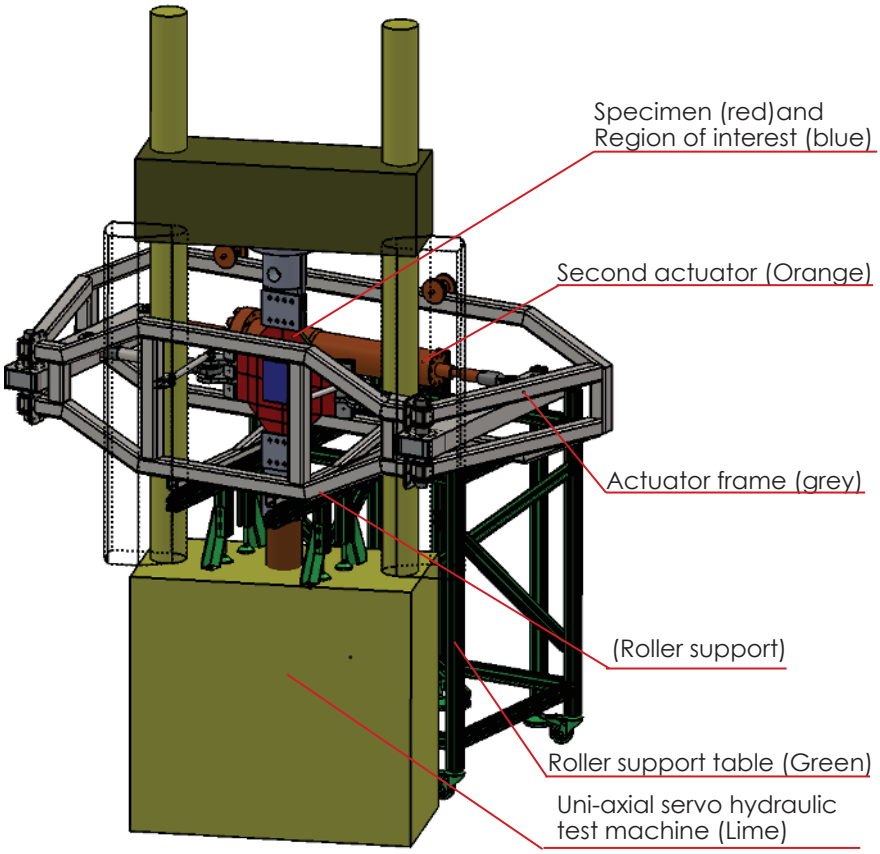

Figure 16. The Biaxial sandwich test rig design

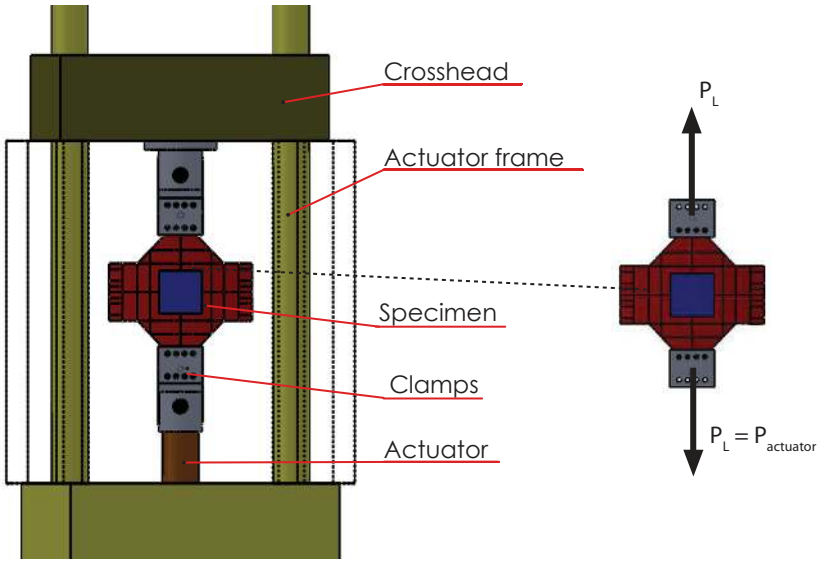

Figure 17. The longitudinal loading frame and free body diagram of the specimen

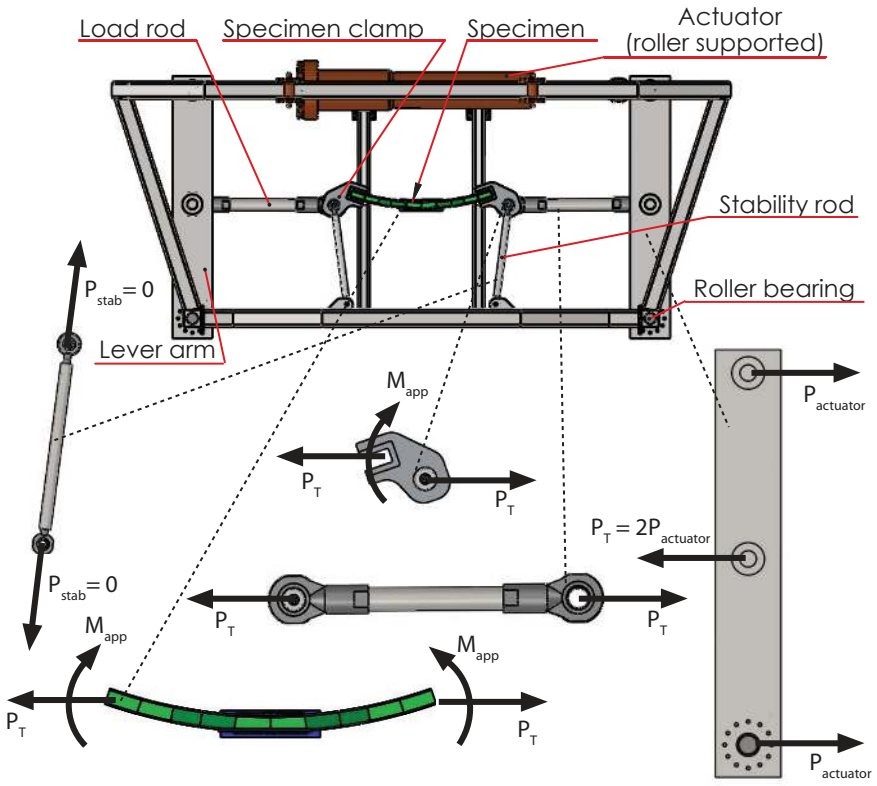

Figure 18. The transverse loading frame and free body diagrams of the specimen and subcomponents

of two lever arms and a roller support for the actuator. This facilitates that the position of the specimen (i.e. the sandwich substructure) remains centred w.r.t. the vertical loading frame during deformation. The specimen clamps are constructed such that the load application points can be offset relative to the centre of the panel. This offset accommodates for the applied bending moment, M_{app}, which at the centre of the panel corresponds directly to $M = kP_T$ shown in Equation (1). The variation of the applied bending moment compared to the bending moment in the centre is only dependent on the curvature of the panel, and hence $M_{app} = kP_T$ if flat panels are considered. Further, two stabiliser rods are introduced to prevent rotational instability wrt. the longitudinal axis. The loading rods are mounted with spherical joints, which compensate for the movement of the centre position in the longitudinal direction that will occur during deformation. Thus, $P_{stab} = 0$, when equilibrium wrt. the chosen deformation configuration is reached since the transverse loading frame will move accordingly. It is important to note that $P_{stab} = 0$ due to the roller support shown in Figure 16, and hence the stabiliser rods do not influence the loading condition applied to the panel. The realised test rig is shown in Figure 19. The loading rods are positioned on the lever arms such that the load capacity of the horisontal actuator is doubled. Thus, the test setup has a maximum capacity of 400 kN for the longitudinal force P_L, and 126 kN for the transverse force P_T. The load

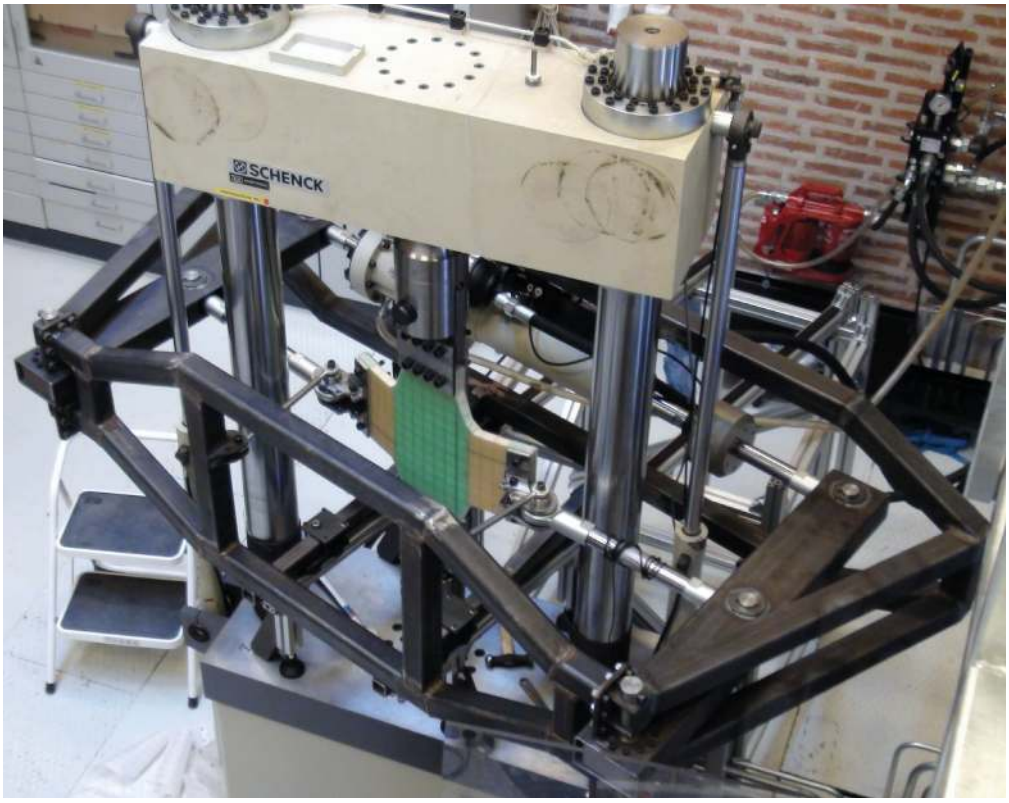

Figure 19. The realised experimental setup

capacities of the actuators provide a setup where the maximum biaxial load ratio is approximately 1/4. The relatively high ratio is chosen in correspondence with the developed specimen design described in the following section. The actuators are controlled by an Instron 8800 controller, which enables quasi-static and fatigue tests in either force or displacement control.

4.1.1. Test specimen design

In addition to the test rig design a specially designed test specimen has been developed. The specimen geometry is cruciform-like, but in addition to this, a detailed laminate design is made to ensure proper load introduction into the gauge zone to avoid premature failure due to end and clamping effects. An example of the produced sandwich panel and its geometry after cutting is shown in Figure 20. The highlighted centre of the panel constitutes the gauge zone, whereas the remaining parts constitute the load introduction sections in the longitudinal and transverse directions, respectively. In principle the material choice and the specimen design can be generic provided that the experimental investigations can be conducted within the defined load envelope (capabilities) of the test rig. However, since the specific blade design consists

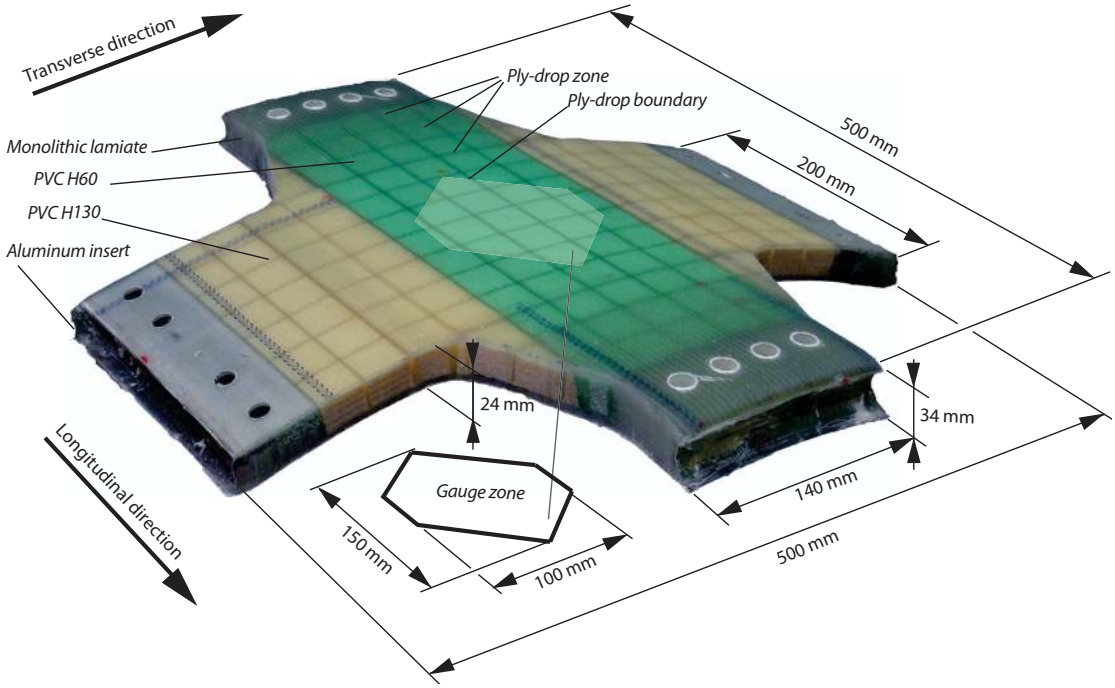

Figure 20. Prepared specimen after cutting and drilling, where the highlighted area constitute the gauge zone

of lay-ups of glass fibre fabric layers and PVC foam infused with an epoxy resin system, the same material and lay-up configurations have been chosen for the test specimens. To limit the use of different glass fabrics, Triax 1200 g/m^2 glass fabric (non-crimp unidirectional glass fibre oriented in 0° (600 g/m^2), +45° (300 g/m^2), and -45° (300 g/m^2)) was used for all plies. The lay-ups for the different regions within the specimen are shown in Figure 21. The stacking-sequence notation indicate the orientation of each ply and the associated subscript nT refers to that n layers of Triax or PVC ($n = 1$ when T or PVC appears without a number) have been used. Since the core material is equally split by the middle surface a bar is put over that term to adopt the notation for a symmetric S lay-up. In the gauge zone a single layer of Triax was used together with the low density grid-scored core (PVC H60), which was the grid-scored core material of particular interest for this study. To obtain the highest stresses and strains in the centre of the specimen (referred to as the gauge zone), a cutout is made in two of the plies used in the centre of the specimen. This reduces the thickness further in the gauge zone, and hence make this region most compliant. Additional reinforcement was added in the longitudinal direction to accommodate for the large longitudinal load component, and a high density foam (PVC H130) was used in the transverse direction to increase the shear strength. Cutouts were made in the sandwich core to make room for a monolithic laminate in the longitudinal clamping zone and an aluminium insert in the transverse clamping zone.

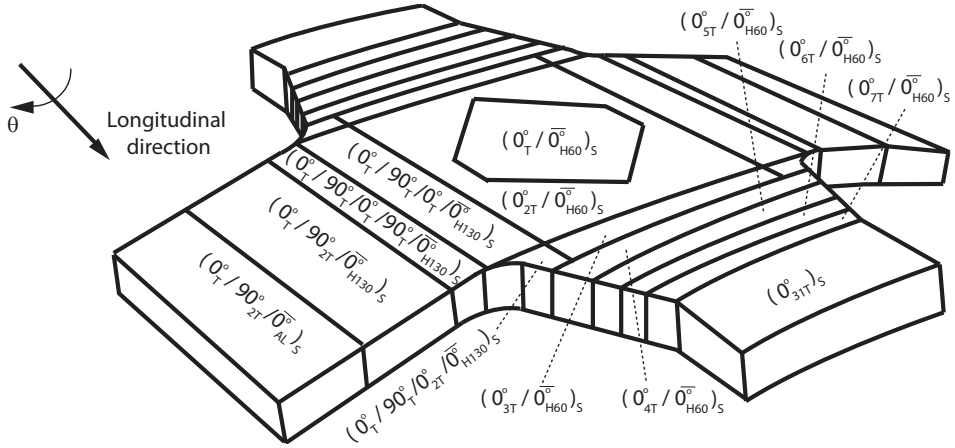

Figure 21. Stacking-sequences for the different regions of the curved sandwich specimen

It is important to note that the developed test specimen configuration displays more complex stress and strain distributions than the idealised model described in Section 3.3.2. The overarching goal when specifying the test specimen configuration was to facilitate failure in the gauge zone, and at the same time develop stress and strain distributions that are comparable to the stress and strain states predicted by the full scale FE model predictions. Consequently, this influences the relationships between the three load components (P_L, P_T and M, see Figure 11), which have to be reestablished for the test specimen design. For that purpose, equivalent to the idealised 3D numerical model shown in Figure 13, an FE model of the developed test specimen configuration has been made, see Figure 22. Since the idealised FE model predictions (cf. Figure

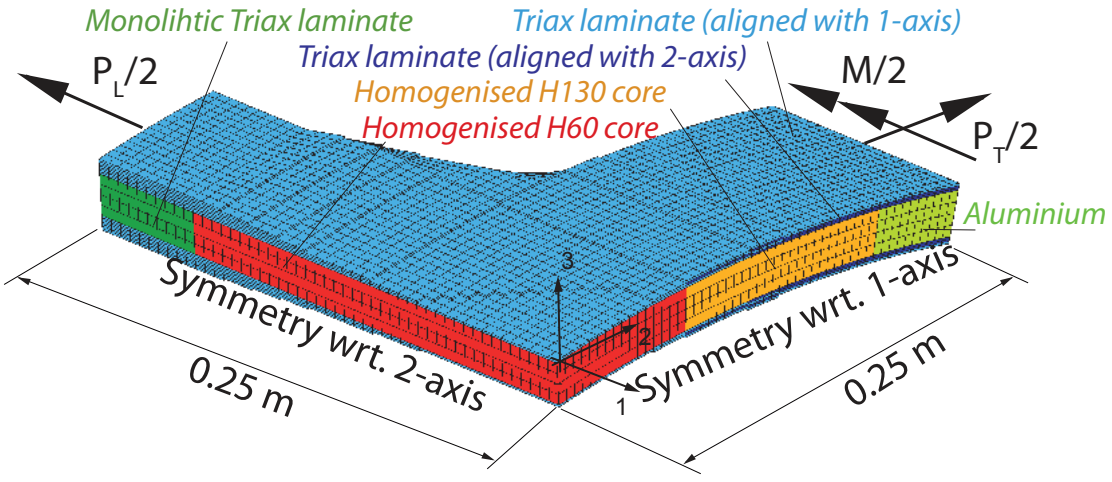

Figure 22. FE model of the test specimen configuration

13) enabled a detailed investigation of the localised load distribution the FE model of the test specimen was simplified

to decrease the computation time. Thus, the homogenised stiffness properties of the foam core and resin bridges were calculated as explained in [16], and symmetry conditions were adopted. The FE model was discretised by 17,000 eight node solid elements in MSC Nastran where the elements for the face sheet use an enhanced assumed strain formulation (solid shell) to stabilise and circumvent locking effects due to high aspect ratios of the elements. Similar to the idealised FE model the present model was chosen only to facilitate linear predictions. The reason for this was that the model has been used to fine tune the established loading conditions, such that the stress and strain distributions obtained from the full scale model can be reproduced within the feasible loading envelope of the chosen test setup. The selection of appropriate local loading conditions is elaborated in the forthcoming.

4.2. Experimental results

In Section 3.3.2 it was found that biaxial in-plane tension or compression loads combined with a bending moment in the curved direction of the panel provide a good representation of the stress and strain states when the blade is subjected to the different global bending loading conditions. In this study three specific quasi-static load scenarios that define the failure behaviour of the grid-scored sandwich panel substructure have been investigated. The analyses and tests have been made for a radius of curvature equal to 750 mm, which is representative for the blade substructure outlined in Figure 1. For all the analysed cases the in-plane loading conditions were chosen such that the transverse in-plane load, P_T, was applied at a fixed ratio compared to the longitudinal in-plane load, P_L. In a similar way the magnitude of the transverse bending moment, M, was specified as a ratio of the transverse in-plane load, P_T. Three different levels of the M/P_T ratio was tested. An overview of the three load cases is shown in Table II, which include one biaxial tension and two biaxial compression loading combinations. The reason for choosing two different magnitudes of the transverse bending

Table II. The three investigated load cases

Load case	$P_T(P_L)$	$M(P_T)$
Biaxial tension with a small bending moment	$P_L/4$	$0.002P_T$
Biaxial compression with a small bending moment	$P_L/4$	$0.004P_T$
Biaxial compression with a significant bending moment	$P_L/4$	$0.008P_T$

moment M for the two biaxial compression cases relates to a change in the observed failure mode. When a relatively small bending moment was applied, failure occurred in the vicinity of the gauge zone ply-drop (see Figure 28), which has no relation to the grid-scoring of the core. Opposed to this, a significantly higher transverse bending moment caused

premature failure of the sandwich core, which triggered a subsequent ultimate failure of the entire sandwich substructure. From the post mortem inspection of the failed specimen, it appears that the core failure initiated as a crack inside a resin bridge in the grid-score on the tensile side of the panel. For the biaxial tension case failure in all cases was initiated in the grid-scored sandwich core in the gauge section of the specimen, even for a small bending moment. The reason for not changing the ratio between the in-plane loading components in the investigations is related to the interpretation of the full scale results. As explained previously, the constrained contraction behaviour was primarily found to relate to Poisson's ratio effects, hence only small changes of the ratio between the two in-plane load components are likely to occur between different blade designs. In comparison to Figure 14, which shows the P_L/P_T ratios predicted by the full scale nonlinear FE model of the blade, it is seen that the in-plane load ratio has been changed significantly from about 1/10 to the value of 1/4 specified for the tests. The reason for this is the layout of the developed test specimen configuration. The outlined relationships between the three load components (P_L, P_T and M) shown in Figures 14, **??**, and 15 were all based on idealised linear FE model predictions. In the test specimens the longitudinal load component is applied such that the in-plane normal stresses increase significantly towards the gauge zone. Thus, a larger transverse force (P_T) has to be applied to reproduce the stress and strain distributions predicted by the full scale FE model. The experimental observations of the three load cases are described in the subsequent sections.

4.2.1. Biaxial tension with a small bending moment

For the biaxial tension load case the moment was applied as $M = 0.002P_T$ where the sign convention follows from Figure 11. As illustrated in Figure 23, the FE model of the specimen has been used to predict the strain distribution through-thickness in the centre of the gauge zone. This is compared with the full scale blade model predictions for the flapwise and edgewise load cases, which generally result in tension in the considered sandwich substructure. Since the strain components over the surface of the substructure vary significantly, as shown in Figure 9, it was decided to compute an average value and then to emulate this distribution in the substructure test. The comparison of strains has been made for $P_L = 60$kN since this results in strain levels that are very close to strain levels obtained for the 300% flapwise and edgewise loading cases (see Figures 3 and 10). The combined global loading condition has been omitted, since it is encompassed by the edge- and flapwise loadings as shown in Figure 14. The transverse strain (ε_2) distribution for the edgewise loading (see Figure 23, red dotted line for ε_2-plot) indicates that a bending moment of opposite direction was present compared to the flapwise loading case (see Figure 23, blue dotted line), but this was not the case. The predictions of the full scale FE model together with the experimental recordings show deformation patterns that contradict this. A possible explanation for this discrepancy is the relatively small bending moment present for this load case combined with the averaging of the strain

components over the surface. Thus, the selected loading combination realised in the test lies somewhere in between the edge- and flapwise loadings. To verify that the predicted local strain distributions are replicated with reasonable accuracy

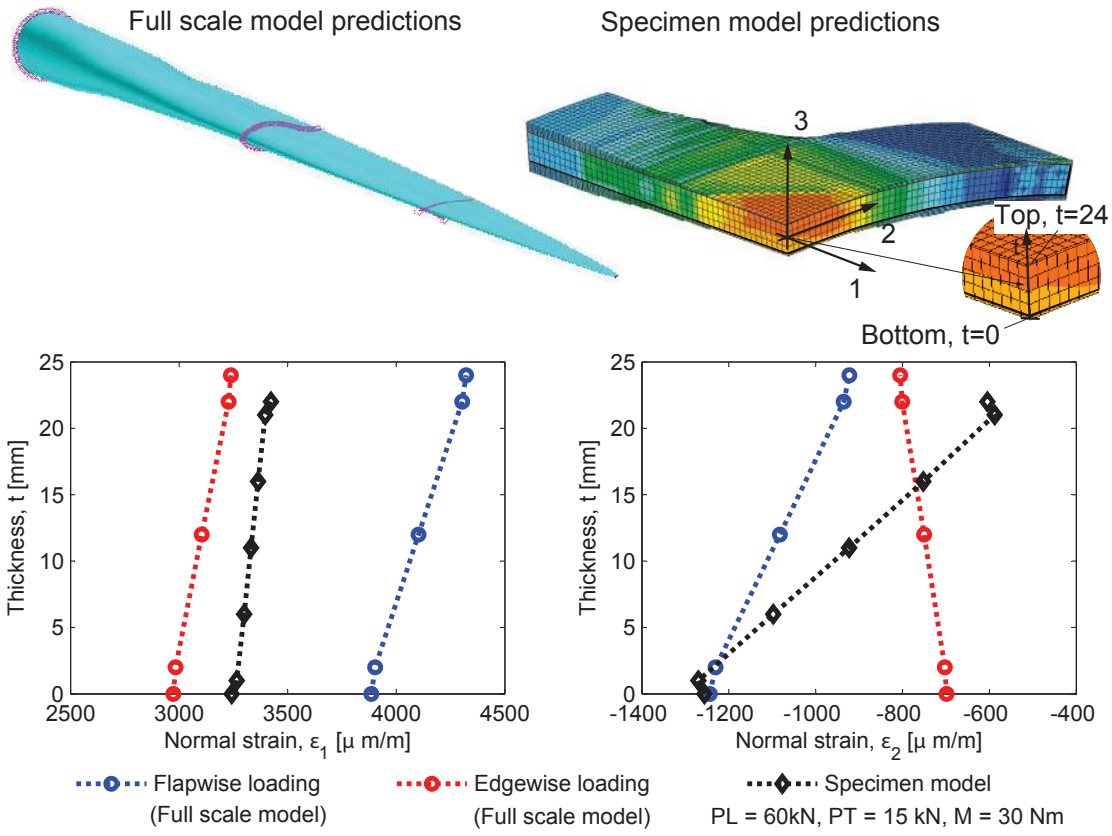

Figure 23. Predicted longitudinal (ε_1) and transverse (ε_2) strain distribution for the case of biaxial tension loading superimposed with a small transverse bending moment

in the test setup, the test specimen was mounted with strain gauges on both sides in the gauge zone. The strain gauges were oriented in the longitudinal and transverse direction, respectively, and hence only the normal strains ε_1 and ε_2 were measured. Figure 24 shows the measured strain response as well as the predictions of the 3D linear model of the test specimen (sandwich substructure). It is seen that the measured response shows a reasonably linear behaviour up to very high loading levels although a slight offset compared to the FE predictions is observed. The test was stopped at $P_L = 250$ kN, which is just before matrix cracking of the face sheets would have occurred. The reason for this is that onset of damage initiation / cracking, although not detectable on the measured strain-load curves, had initiated in the resin grid around $P_L = 90$ kN corresponding to 5000 μm/m strain in the longitudinal direction. The onset of failure (cracking and debonding) was visualised as white spots on the surface of the sandwich substructure. As shown in Figure 25, a subsequent

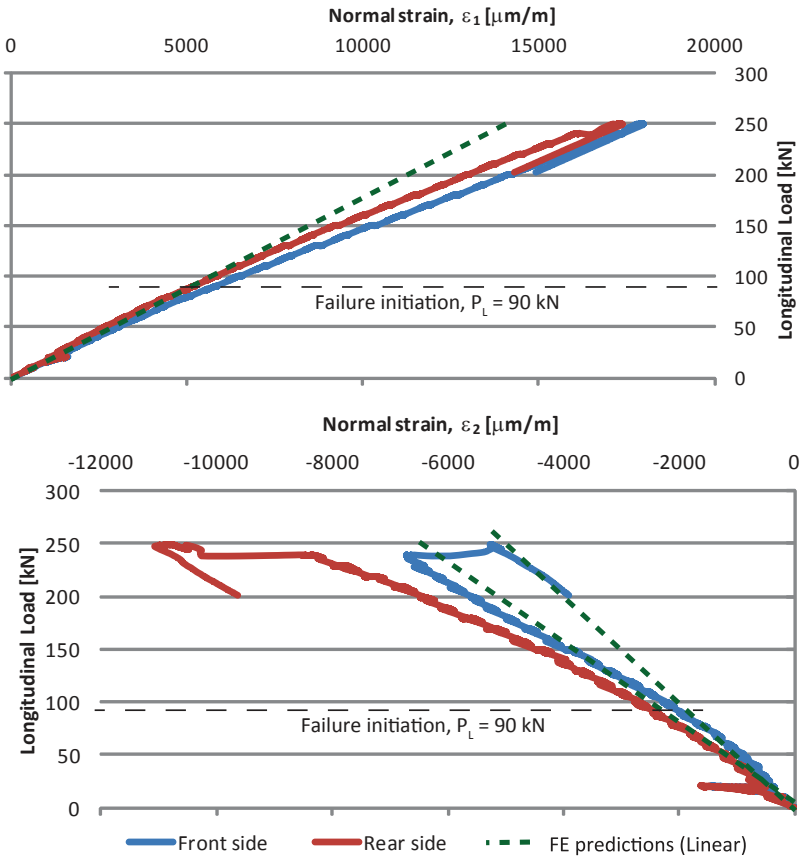

Figure 24. Measured longitudinal (ε_1) and transverse (ε_2) strain distribution compared to the linear FE predictions

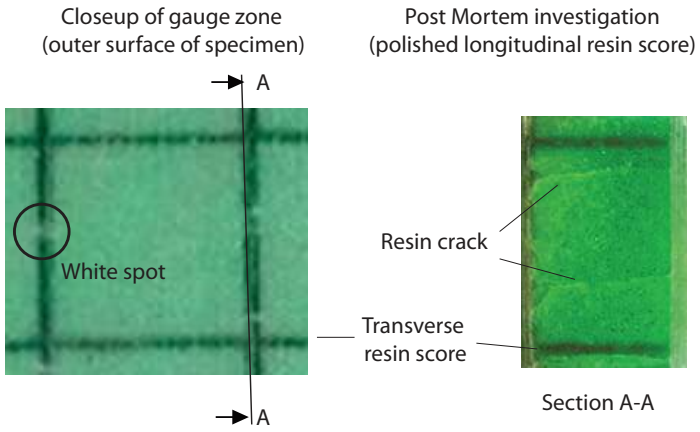

Figure 25. Onset of crack formation in the resin grid observed for the biaxial tension load case

post mortem investigation revealed that the observed whitening was a result of a through-thickness cracking in the resin grid (Section A-A) in situ the core.

4.2.2. Biaxial compression with a small bending moment

For the first biaxial compression case the moment was applied as $M = 0.004P_T$. This load case displayed the failure mode which was observed also for the same biaxial compression cases but with smaller values of the transverse bending moment imposed. Comparing the through-thickness normal strain distributions obtained from the 3D and linear substructure model and the full scale nonlinear blade analysis, shown in Figure 26, it is seen that the imposed transverse bending moment results in a transverse normal strain distribution, which is more severe than what is actually present in the blade. The strain gauge measurements and the linear substructure FE model predictions are shown in Figure 27. Opposite

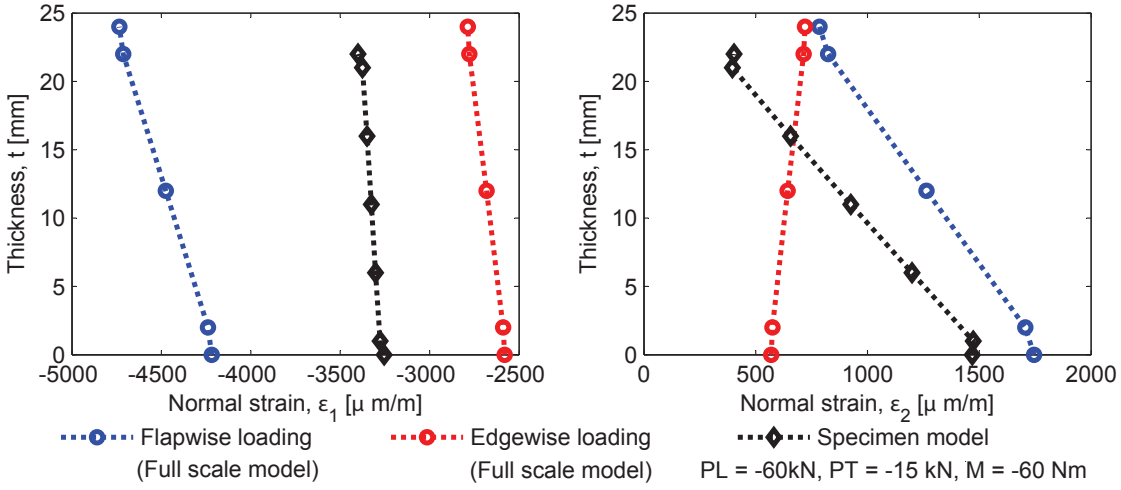

Figure 26. Predicted longitudinal (ε_1) and transverse (ε_2) strain distribution for the case of biaxial compression superimposed with a small transverse bending moment

to the biaxial tension load case significant nonlinear behaviour occurs when P_L exceeds a level of about 60kN. Thus, as a minimum a geometrically nonlinear FE model would be required to capture the load response for this case. However, as the scope of the present study was to investigate the occurrence of failure, rather than to provide an accurate prediction of the deformation behaviour, it is assessed that extrapolated linear predictions will be sufficiently accurate, since these will still indicate the relationship between the governing local loads in the wind turbine blade. No failure related to the grid-scored core was observed despite the presence of a relatively large transverse bending moment which led to substantial straining in the transverse direction. Ultimately, failure of the face sheet occurred in the vicinity of the ply-drop for a P_L value of approximately -130kN , which is shown in Figure 28.

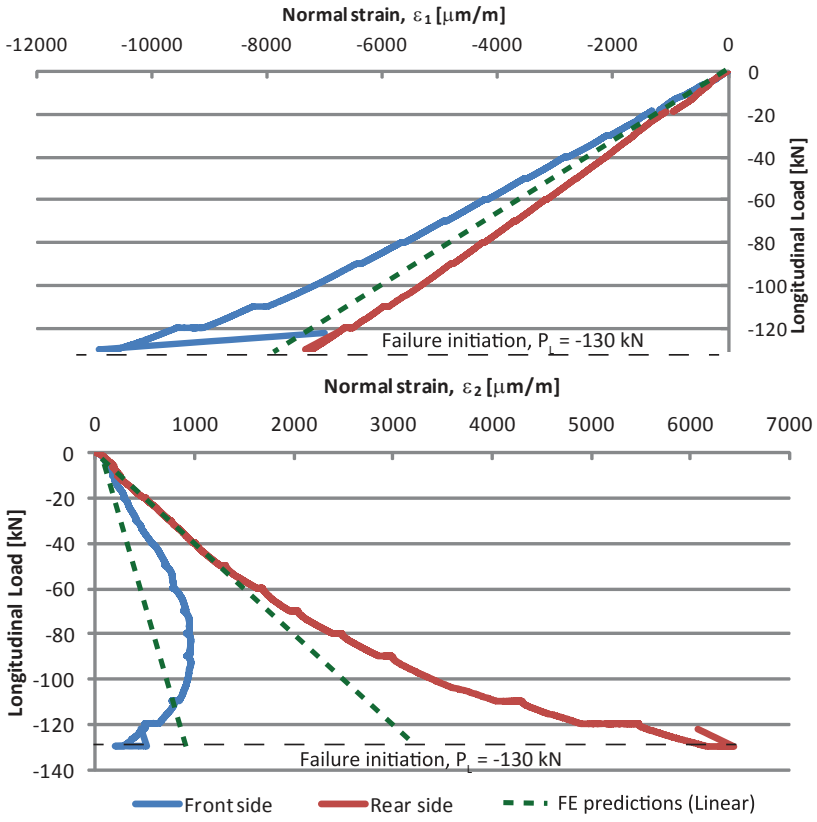

Figure 27. Measured strain distribution compared to the linear FE predictions

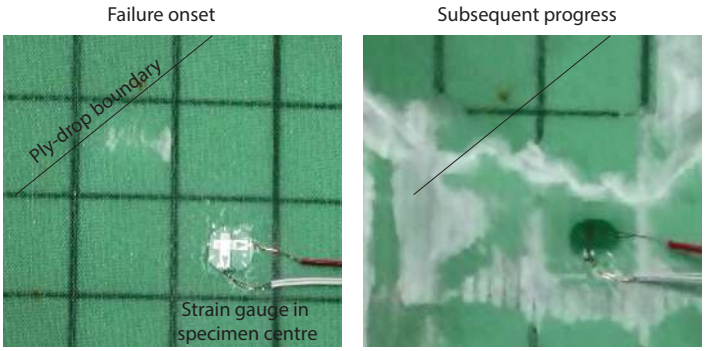

Figure 28. Onset of face sheet failure in the vicinity of the ply drop as consequence of the compression loading case

4.2.3. Biaxial compression with a significant bending moment

For the second biaxial compression case a relatively significant transverse bending moment loading was defined by $M = 0.008P_T$. This corresponds to twice the value of the transverse bending moment imposed in the previous case. This is also reflected in Figure 29, which shows the through-thickness normal strain distributions in the longitudinal and

transverse directions predicted from the global blade model (flapwise and edgwise loads), and the local substructure FE model with biaxial compression superimposed with significant bending moment loading. The transverse normal strains (ε_2) are seen to be very large, whereas the longitudinal strains are predicted to have the same distribution as for the previous case (cf. Figure 26). The measured strain vs. load data displayed in Figure 30 show that failure for this case occurred at a lower

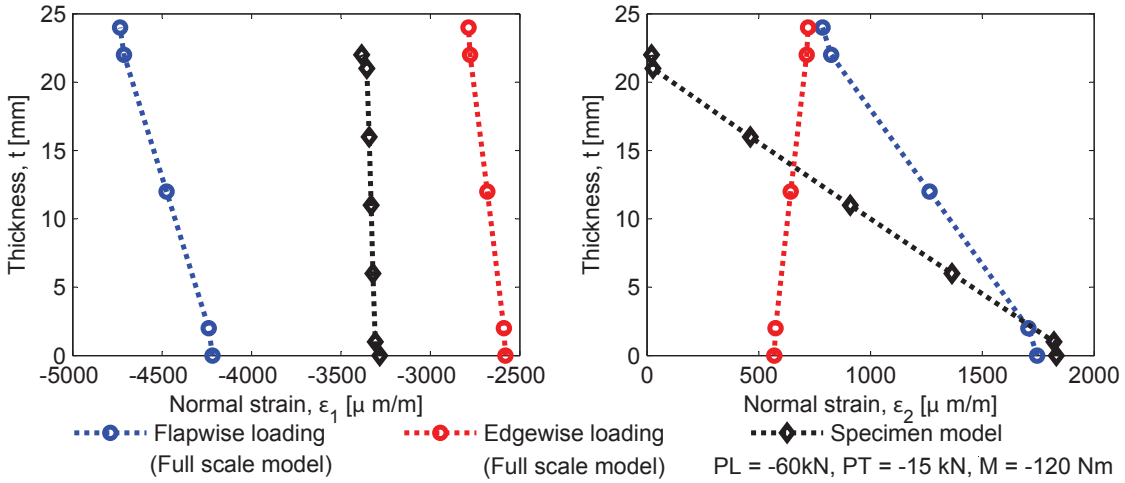

Figure 29. Predicted longitudinal (ε_1) and transverse (ε_2) strain distribution for the case of biaxial compression superimposed with significant transverse bending moment

longitudinal load level (P_L approx. -110kN) than for the previous case. Similar to the previous case, nonlinear behaviour in the transverse direction was observed. The reason for the lower load carrying capacity can be related to a change in failure mode, which for this case did not occur in the vicinity of the ply-drops but rather due to fracture (cracking) of the resin grid in the transverse direction. As shown in Figure 31, failure initiation in the transverse resin bridge was observed on the rear side of the panel. In Figure 31 the resin grid appears almost translucent. The reason for this is that the specimen was monitored using a high-speed camera during the testing, and this camera required a significant amount of illumination on the front side of the specimen. This allowed detection of the onset of failure (i.e. crack development) in the resin grid, which in this case was observed as the first failure event. Subsequently, the failure initiation and propagation in the resin resulted in a circular delamination of the face sheet seen on the front side of the specimen. The subsequent progressive failure sequence occurred very rapidly. Since the face sheet loaded in biaxial compression delaminated from the core, face sheet wrinkling and debonding occurred leading to a total loss of load carrying capability of the sandwich substructure specimen.

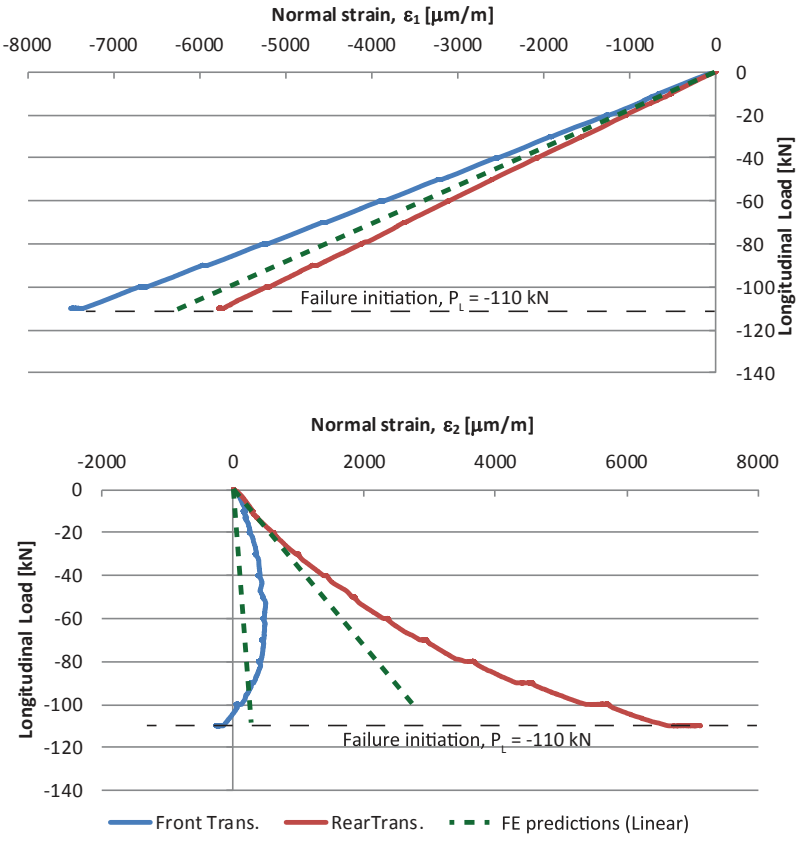

Figure 30. Measured strain distribution compared to the linear FE predictions

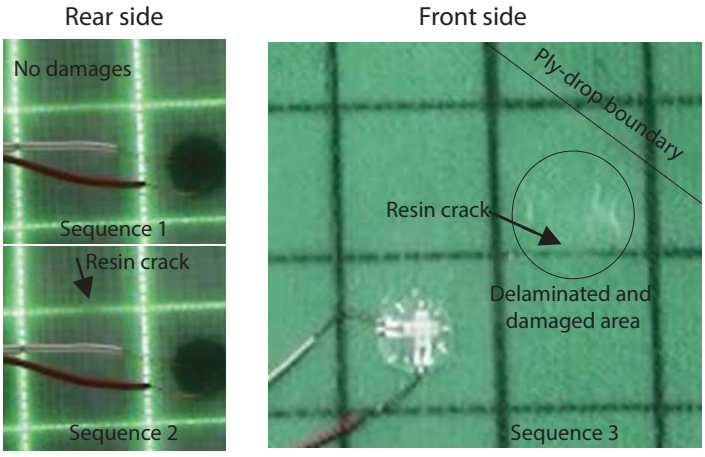

Figure 31. Initiation of fracture in the resin grid for the case of biaxial compression loading superimposed with a significant transverse bending moment

5. RECOMMENDATIONS ON THE USE OF GRID-SCORED SANDWICH PANELS

Based on the experimental observations and the conducted FE analyses, a set of recommendations can be suggested for the use of grid-scored sandwich panels in the aerofoils of wind turbine blades. To propose more generic design guidelines for the overall blade structure, experimental evidence considering the design parameters outlined in Section 4 would be required. However, the investigation presented in this study has identified critical load combinations and magnitudes for the grid-scored sandwich substructure, which may cause premature failure. Based on these observations the following recommendations for the use of grid-scored sandwich panels in the aerodynamic shells of wind turbine blades can be outlined:

Tension loaded panels: In any biaxial tension loading scenario, the normal strain can lead to fracture in the resin grid of the slits in the same direction as the normal strain component, which in this case will be in the longitudinal blade direction.

Compression loaded panels: In cases where a transverse bending moment of significant amplitude acts in combination with a biaxial state of compression loading, cracking in the resin grid of the core slits may be induced in the same direction as the bending moment.

Special awareness is recommended for sandwich panels loaded in biaxial compression, as the onset of cracking in the resin grid combined with the high compressive stresses results in a dramatic failure sequence leading to face-core debonding, face sheet buckling and total loss of stiffness. The occurrence of such failure phenomena will primarily take place in the presence of either significant ovalisation (Brazier effect as discussed) of the blade, or due to a low chordwise stiffness of the blade. Furthermore, localised deformations induced by stiffness changes e.g. interconnections between the aerofoil shell and the shear webs may result in local loading combinations similar to the ones outlined, hence potentially leading to a premature failure.

6. DISCUSSION

The present paper outlines the potential benefits of developing a high fidelity substructure test methodology over conventional uniaxial or simplified coupon tests. First of all, the presence of multiaxial loading scenarios that are more realistic than uniaxial loading states can be investigated in relation to failure. This in combination with testing specimen configurations that are similar to the actual geometry in situ the structure, provides the opportunity to observe the load response leading to failure in detail, and from this to develop a comprehensive understanding of the real failure behaviour.

The study presented in this paper has been focused on the analysis of the influence of grid-scoring in foam cored sandwich panels used in aerofoil shells for wind turbine blades. The developed biaxial sandwich substructure tests have shown that a specific combination of loading and geometric configurations lead to high risk of premature failure under realistic loading conditions. Similar results could not have been deduced from uniaxial standard tests. More importantly, the proposed multiaxial substructure testing methodology can be used to inform and calibrate high fidelity nonlinear FE analyses in a way, that could otherwise only be achieved through very costly full scale blade structure tests. Thus, albeit the cost and effort of developing a high fidelity substructure test facility are substantial in comparison with simple uniaxial coupon testing, the added value may in many cases be assessed as justified. A further perspective of the multiaxial substructure test facility discussed in this paper is the investigation of the fatigue behaviour on the substructure level. It is of utmost importance to understand the fatigue limits of the blade materials and subcomponents, as wind turbine blades have normally been designed to a service life of 20 years. The multiaxial sandwich substructure test facility developed has been designed and commissioned also for fatigue testing, and this will be pursued in the continuation of this work.

7. CONCLUSION

Based on combined numerical and experimental characterisation of the full scale load response of a wind turbine blade, and subsequent substructure test development, the present study illustrates how a full scale test can be translated into a more detailed subcomponent test without significantly compromising the in situ loading state. This is particularly useful when the objective is to observe and understand the failure initiation and progression under realistic (multiaxial) loading scenarios, as well as in situations where test to failure of the full scale structure is not possible to the same extent. Figure 32 shows a road map in terms of the steps taken from beginning to end of this study to develop a high fidelity experimental substructure test rig for grid-scored sandwich panels used in wind turbine blades. The road map is presented in a generic form, and hence applicable to substructure testing of other parts in composite wind turbine blades or other composite structures. As shown, four steps are taken to facilitate the detailed experimental characterisation. Step 1 involves the characterisation of the full scale structure. Here it is assumed (assumptions in italic format) that experimental evidence for the region of interest is sufficient to validate the numerical model, which for most composite structures must facilitate geometrical nonlinear predictions. Step 2 involves the interpretation of deformation behaviour and establishment of suitable loading conditions. An idealised model can show beneficial to get more detailed stress/strain predictions and validity of local linearity assumptions can be investigated. The established loading conditions facilitate the development and realisation of the high fidelity test rig in Step 3. The basic assumption for the test rig is that is facilitates realistic loading conditions. This

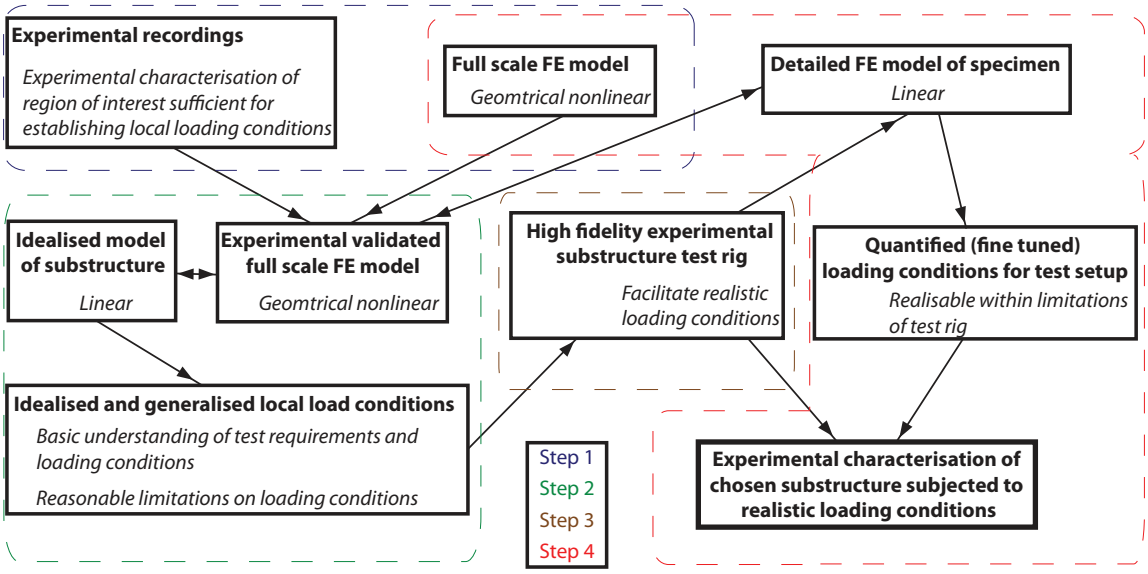

Figure 32. Road map of the present study

is validated in Step 4 where a detailed model of the specimen is compared with the validated full scale predictions. Further, the comparison allows a fine tuning of the desired loading conditions provided these are realisable within limitations of the test rig. Finally, the procedures in Step 4 allow the detailed experimental characterisation of the chosen substructure.

For the present study the final step has enabled a closer investigation of the failure phenomena occurring when the substructure is subjected to loading conditions derived from the full scale numerical modelling. For the particular grid-scored sandwich substructure investigated, which represents a part of the aerodynamic outer shell of a wind turbine blade, it has been found that the tension-tension-bending load case leads to damage initiation in the resin grid. For the compression-compression-bending load case, face sheet delamination and subsequent wrinkling were observed, as a result of onset of cracking in the transverse resin slits in the core. The progressive series of failure phenomena were triggered by a significant transverse bending moment occurring due to cross section ovalisation. This indicates that special awareness of this load component in combination with biaxial compression is recommended when using grid-scored sandwich configurations in the aerodynamic shell of wind turbine blades.

ACKNOWLEDGEMENT

The work presented is part of an Industrial PhD project carried out in collaboration between SE Blades Technology, Denmark and the Department of Mechanical and Manufacturing Engineering, Aalborg University, Denmark. The project

has received partial sponsorship from the Danish Agency for Science, Technology and Innovation. The support is gratefully acknowledged.

REFERENCES

1. Zienkiewicz OC, Taylor RL. *The finite element method for solid and structural mechanics*, vol. 2. Butterworth-Heinemann, 2005.
2. Sutton MA, Wolters WJ, Peters WH, Ranson WF, McNeill SR. Determination of displacements using an improved digital correlation method. *Image and Vision Computing* 1983; **1**(3):133–139.
3. Chu TC, Ranson WF, Sutton MA. Applications of digital-image-correlation techniques to experimental mechanics. *Experimental mechanics* 1985; **25**(3):232–244.
4. Zenkert D. *An introduction to sandwich construction*. Engineering Materials Advisory Services, 1997.
5. Hinton MJ, Kaddour AS, Soden PD. A comparison of the predictive capabilities of current failure theories for composite laminates, judged against experimental evidence. *Composites Science and Technology* 2002; **62**(12-13):1725–1797.
6. Overgaard LCT, Lund E, Thomsen OT. Structural collapse of a wind turbine blade. part a: Static test and equivalent single layered models. *Composites Part A: Applied Science and Manufacturing* 2010; **41**(2):257–270.
7. Overgaard LCT, Lund E. Structural collapse of a wind turbine blade. part b: Progressive interlaminar failure models. *Composites Part A: Applied Science and Manufacturing* 2010; **41**(2):271–283.
8. Ostergaard MG, Ibbotson AR, Roux OL, Prior AM. Virtual testing of aircraft structures. *CEAS Aeronautical Journal* 2011; **1**(1-4):1–21.
9. Johannes M, Jakobsen J, Thomsen OT, Bozhevolnaya E. Examination of the failure of sandwich beams with core junctions subjected to in-plane tensile loading. *Composites Science and Technology* 2009; **69**(9):1447–1457.
10. Johannes M, Thomsen OT. Localised effects in sandwich structures with internal core junctions: Modelling and experimental characterisation of load response, failure and fatigue. Springer, 2010; 229–277.
11. Ahmad S, Irons BM, Zienkiewicz OC. Analysis of thick and thin shell structures by curved finite elements. *International Journal for Numerical Methods in Engineering* 1970; **2**(3):419–451.
12. MacNeal RH. Perspective on finite elements for shell analysis. *Finite elements in analysis and design* 1998; **30**(3):175–186.

13. MacNeal RH, Wilson CT, Harder RL, Hoff CC. The treatment of shell normals in finite element analysis. *Finite elements in analysis and design* 1998; **30**(3):235–242.

14. Laird DL, Montoya FC, Malcolm DJ. Finite element modeling of wind turbine blades. *43rd AIAA Aerospace Sciences Meeting and Exhibition, Reno, Nevada*, 2005.

15. Brazier LG. On the flexure of thin cylindrical shells and other" thin" sections. *Proceedings of the Royal Society of London. Series A* 1927; **116**(773):104–114.

16. Thomsen OT, Larsen J. Simplified rule of mixtures approach for the accurate estimation of the elastic properties of grid-scored polymer foam core sandwich plates. ISBN: 978-972-8953-23-2, 2008; 261–274.